Influence of montmorillonite/carbon nanotube hybrid nanofillers on the properties of poly(lactic acid)

Olawale Monsur Sanusi, Abdelkibir Benelfellah, Lazaros Papadopoulos, Zoi Terzopoulou, Lamprini Malletzidou, Isaak Vasileiadis, Konstantinos Chrissafis, Dimitrios Bikiaris, Nourredine Aït Hocine

Influence of montmorillonite/carbon nanotube hybrid nanofillers on the properties of poly(lactic acid)

Olawale Monsur Sanusi[a,b,*], Abdelkibir Benelfellah[a,c], Lazaros Papadopoulos[d], Zoi Terzopoulou[d], Lamprini Malletzidou[e], Isaak G. Vasileiadis[e], Konstantinos Chrissafis[e], Dimitrios N. Bikiaris[d,*], Nourredine Aït Hocine[a,*]

[a] *INSA CVL, Univ. Tours, Univ. Orléans, LaMé, 3 rue de la Chocolaterie, CS 23410, 41034 Blois, Cedex, France*

[b] *Department of Mechanical Engineering, Federal University Oye-Ekiti, Ekiti, Nigeria*

[c] *DRII, IPSA, 63 boulevard de Brandebourg, 94200 Ivry-Sur-Seine, France*

[d] *Department of Chemistry, Laboratory of Polymer Chemistry and Technology, Aristotle University of Thessaloniki, GR-541 24, Thessaloniki, Greece*

[e] *Department of Physics, Aristotle University of Thessaloniki, GR-541 24, Thessaloniki, Greece*

[*]Corresponding authors.

Email addresses: sanuthwale@gmail.com (O. M. Sanusi); dbic@chem.auth.gr (D. N. Bikiaris); nourredine.aithocine@insa-cvl.fr (N. Aït Hocine)

ABSTRACT

Multi-walled carbon nanotube (MWCNT) and montmorillonite (Mt) are used as reinforcing fillers in polymers. Achieving homogeneous distribution of the reinforcing nanoparticles without agglomerates in polymeric matrices continues to be an important topic in materials science. In this study, hybrid Mt/MWCNT nanofiller was prepared after determining the most stable composition with the help of dynamic light scattering (DLS). The hybrid Mt/MWCNT was characterized via X-ray diffraction (XRD) and Fourier-transform infrared (FTIR) spectroscopy. The Mt/MWCNT hybrid fillers were incorporated in poly(lactic acid) (PLA) at concentrations of 0.5, 1 and 2 wt%, by a two-step procedure of solution and melt mixing, and their physicochemical, thermal, mechanical and morphological properties were evaluated. The physicochemical studies suggested strong hybrid-polymer interaction. The structural analyzes confirmed synergy between nanoclay and carbon nanotubes in achieving homogeneous dispersion of Mt/MWCNT nanoparticles in the PLA matrix. The thermal characterizations depicted that the Mt/MWCNT hybrid nanofillers synergistically restricted the PLA segment motions and promoted the crystallization of the polymer matrix. The mechanical properties of PLA/Mt/MWCNT nanocomposites were improved, confirming the reinforcing effect of the Mt/MWCNT hybrid on PLA matrix.

Keywords: Poly(lactic acid), montmorillonite, carbon nanotubes, nanocomposite, hybrid

1. Introduction

Polymer nanocomposites gain increasing interest in advanced engineering applications such packaging, sports, military, energy and automobile, due to their multi-functional properties (Ramírez-Herrera et al., 2019). For ecological protection, more research attention is directed towards polymers that are biocompatible and biodegradable, like poly(lactic acid) (PLA). PLA is an aliphatic polyester, commercially sourced from renewable agricultural produce, and known for its easy processability by any of the conventional thermoplastic processing techniques, degradability to natural products and good mechanical properties (Liu et al., 2019; Yang et al., 2011; Katiyar et al., 2010). The use of nanoparticles in polymers to develop composites remains highly attractive because of their large interfacial area, low percolation threshold, and commensurate size scale between nanoparticles (Francisco et al., 2018). All these features translate to high mechanical properties, thermal and electrical conductivity, flame retardancy, chemical resistance and decreased permeability of nanocomposites, which are the desirable characteristics for engineering applications (Francisco et al., 2018; Bhattacharya, 2016). Within the previous decade, montmorillonite (Mt) and carbon nanotubes (MWCNTs) remain the leading and most studied nanofillers reported to impact superior properties in various polymeric matrices (Sanusi et al., 2020a; Anbusagar et al., 2018). Therefore, researchers explore the synergistic properties of Mt and MWCNT in polymers (Ma et al., 2007; Hapuarachchi and Peijs, 2010; Geng et al., 2012; Khajehpour et al., 2014; Pandey et al., 2014; Song, 2016; Hosseini and Yousefi, 2017) and blends (Zhu et al., 2020; Al-Saleh, 2015; Chiu, 2017). This is to earnest both of their extraordinary individual properties, reducing the percolation threshold as well as addressing the limitation of each of the two prominent nanofillers (Bilotti et al., 2013). MWCNT typically forms stabilized aggregates attributed to high hydrophobicity, making its dispersion exceedingly difficult (Sianipar et al., 2017; Barrau et al., 2011), while the stacking of Mt

platelets and its incompatibility with common hydrophobic polymers are the common nanoclay challenges (Madaleno et al., 2013; Sibeko, 2012).

In some studies, the two nanofillers were physically added to polymers by solution mixing (Azam and Samad, 2018) or melt mixing (Al-Saleh, 2017; Stern et al., 2018). Yet, agglomerates of the nanofillers in the matrices persisted, related among others, to the increase of filler content in matrix (Azam and Samad, 2018). Recently, Mumtazah et al. (2019) prepared Mt/MWCNT hybrid nanofiller using a sol-gel method with strong acids, in elevated temperatures, to reinforce Chitosan/phthalic anhydride. Such a method constantly raises environmental and hazard concerns because of the acids and energy consumption involved (Koo, 2016).

Growth of MWCNT with catalytic chemical vapor deposition (CCVD) over metal ion-exchanged Mt platelets is another method of preparing preformed Mt/MWCNT hybrid filler to improve polymer properties (Manikandan et al., 2012). The growth of MWCNT over Mt leads to pre-exfoliation of the Mt's internal structure, which facilitates its dispersion in the polymer matrix (Madaleno et al., 2013). Thus, incorporation of CCVD Mt/MWCNT nanofillers in polymers attracts research gains. Santangelo et al. (2011) reinforced PLA with CCVD Mt/MWCNT and achieved enhanced sorption and electrical conductivity in 6-9 orders of magnitude. Gorrasi et al. (2013) reinforced PLA with CCVD Mt/MWCNT and reported less elastic modulus degradation against UV irradiation time compared with neat PLA. Madaleno et al. (2013) also utilized CCVD Mt/MWCNT to develop polyurethane nanocomposite foam, all the composites attained improved compressive strength and thermal stability over the neat matrix. Manikandan et al. (2012) utilized CCVD-prepared Mt/MWCNT fillers to achieve defect-free homogenous Nafion nanocomposite for fuel cell applications. Zhang et al. (2006) incorporated CCVD-prepared Mt/MWCNT into polyamide-6 (PA6), tensile modulus and strength were significantly enhanced by 289% and 153%,

99 respectively. Homogenous dispersion of CCVD Mt/MWCNT and strong adhesion with the
100 polymer, resulting in enhanced mechanical properties of the nanocomposite, were reported.
101 Gorrasi et al. (2014) reported thermal stability, mechanical and electrical properties
102 enhancement in poly(ethylene terephthalate) reinforced with CCVD Mt/MWCNT. Enotiadis
103 et al. (2013) also incorporated Mt/MWCNT in polystyrene-b-poly(isoprene)-b-polystyrene
104 and improved mechanical properties were reported, compared to neat triblock polymer and
105 clay/polymer nanocomposite. However, the CCVD Mt/MWCNT hybrid nanofillers is often
106 said to accelerate thermal degradation rates in the resulting nanocomposites. Most of the
107 studies attributed this drawback to the high thermal conductivity nature of metal particle
108 residues that are usually utilized in exfoliating clay during CCVD (Madaleno et al., 2013;
109 Terzopoulou et al., 2016; Sanusi et al., 2020a). Furthermore, CCVD requires high-energy
110 consumption, use of harmful chemicals, and the process is quite complex (Madaleno et al.,
111 2012; Manikandan et al., 2012; Manikandan et al., 2013).
112 Lately, Wang et al. (2009) dispersed MWCNT in Mt aqueous dispersion before adding
113 poly(ethylene oxide) to form a ternary nanocomposite. Young's modulus, strength at break
114 and elongation of the nanocomposite were reported to be significantly improved. Ma et al.
115 (2019) adopted the same approach by dispersing MWCNT in Mt aqueous dispersion to form
116 Mt/MWCNT hybrid solution. Hydrophobic poly(ether ether ketone) (PEEK) was then mixed
117 with the hybrid aqueous dispersion to form a coating over the PEEK masterbatch. They
118 reported 48% storage modulus enhancement but with reduction in toughness, which was
119 attributed to lack of diffusion of the matrix into the interlayer space of Mt. Levchenko et al.
120 (2011) adopted freeze-drying in preserving the swelling agent (cetyl-trimethyl ammonium
121 bromide) within intercalated Mt, before physical incorporation of MWCNT in polypropylene
122 by melt-mixing. Hence, lyophilization of Mt/MWCNT aqueous dispersions is an efficient and

123 simple method for preparing Mt/MWCNT hybrid nanoparticles, which improves the
124 intercalation of polymeric chains into the layers of Mt.

125 Most recently, Bai et al. (2020) adopted the freeze-drying method to prepare different
126 formulations of functionalized MWCNT:Mt hybrids ((1:1), (1:2), (1:4)) for reinforcing PLA.
127 The elongation at break increased from 5.9% for PLA to 87.3% for PLA reinforced with
128 MWCNT:Mt hybrid in proportion of 1:2 (PLA/MWCNT:Mt (1:2)). The maximum modulus
129 and ultimate strength reached 4.3 GPa and 75.6 MPa, respectively, for the PLA/MWCNT:Mt
130 (1:4) nanocomposite compared to the respective 3.2 GPa and 74.2 MPa for neat PLA.
131 Meanwhile, only nanocomposite reinforced with 1:1 of MWCNT:Mt hybrid had significant
132 enhancement in the thermal stability. Well distribution of the freeze-dried hybrid
133 nanoparticles was reported to be responsible for the properties improvement.

134 In this work, Mt/MWCNT hybrid nanofillers were prepared by ultrasonication and
135 lyophilization technique, and then incorporated in poly(lactic acid) (PLA) via solution casting
136 followed by melt mixing, to study their effects on the properties of PLA. To the best of our
137 knowledge, besides the work by Bai et al. (2020) described above, PLA nanocomposites
138 incorporated with freeze-dried Mt/MWCNT hybrid fillers are uniquely reported. Different
139 from the work of Bai et al. (2020), it is worth noting that three kinds of Cloisite Mt (Mt Na^+,
140 Mt 10A and Mt 20A) and two MWCNT (pristine and functionalized) have been studied in
141 this research, and the most stable Mt/MWCNT hybrid formulation has been selected in
142 achieving nanocomposites. As against chemically functionalized MWCNT that may pose
143 environmental hazard, this research identified the optimal Mt/MWCNT hybrid formulation
144 using pristine MWCNT. In addition, this work presented a detailed structural characterization
145 of the selected Mt/MWCNT hybrid treated by lyophilization in relation with its constituents.
146 Thereafter, the influence of the mass fraction of the selected hybrid nanoparticles on the
147 structure, physicochemical, crystallization, thermal and mechanical properties of PLA was

analyzed. Meanwhile, though thermal study was reported by Bai et al. (2020), the work focused deeply on the relations between morphology and mechanical properties of PLA reinforced with Mt/MWCNT hybrid, by varying concentration of surface compatabilized Mt (1.34TCN Nanocor) over a fixed mass of carboxyl functionalized MWCNT.

2. Materials and methods

2.1. Materials

Poly(L-lactic acid) (PLA) (Ingeo™ Biopolymer 3052D) matrix used in the work was supplied by Plastika Kritis S.A., with molecular weight Mw = 63.090 g/mol and intrinsic viscosity ŋ = 1.055 dL/g. Three different Cloisite® montmorillonite (Mt) nanoclay types were used: Mt Na^+, Mt 10A and Mt 20A, which correspond to unmodified Mt, dimethyl benzyl hydrogenated tallow quaternary ammonium (2MBHT) modified Mt, and dimethyl hydrogenated tallow quaternary ammonium (2MHT) modified Mt, respectively. These nanoclays are produced by Southern Clay Products, Inc. Ganzales, USA. Fig. 1 presents the structures of the modifiers for Mt 10A, Mt 20A and the structure of tallow. Multi-walled carbon nanotubes (MWCNT) and functionalized multi-walled carbon nanotubes (MWCNT-f) with 5% -NH_2 were used as the second nanofillers. The nanotubes are produced by Glonatech SA, Athens, Greece with average diameter of 15±5 nm, length > 5 μm and bulk density of 0.2 g/cm^3. Reagent-grade dichloromethane (CH_2Cl_2) was supplied by Scharlab S.L. Spain.

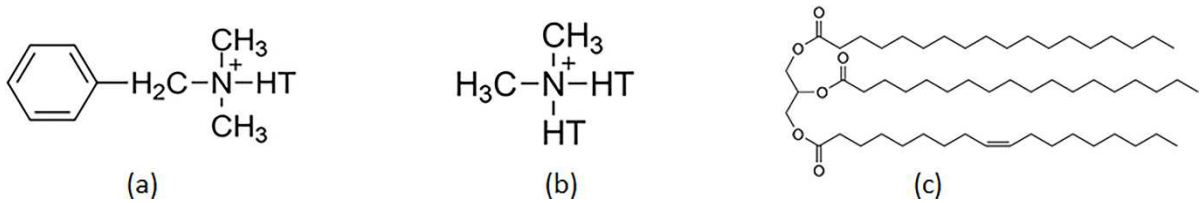

Fig. 1. Chemical structure of (a) dimethyl benzyl hydrogenated tallow quaternary ammonium (2MBHT); (b) dimethyl hydrogenated tallow quaternary ammonium (2MHT); (c) HT - tallow.

2.2. Optimization of hybrid filler composition

The stability and zeta potential (ζ-potential) of different types of Mt (Mt Na^+, Mt 10A and Mt 20A) and MWCNT (CNT, CNT-f) as well as different Mt/MWCNT mass ratios were examined to choose the optimum composition of the hybrid Mt/MWCNT nanofiller. First, an Mt aqueous dispersion was prepared by stirring and ultrasonication (UP100H Ultrasonic Processor Hielscher Ultrasound Technology, Germany) for 5 min. Afterwards, appropriate quantity of MWCNT was added in the Mt dispersion, stirred and ultrasonicated until there were no visible aggregates. The final concentration of the dispersions was 1 mg/mL and the Mt/MWCNT mass ratios tested were 1:1, 2:1 and 4:1 (Table 1). At varying time intervals, photographs of the sedimentation process were captured to monitor the suspension stability. The colloidal stability of the prepared Mt/MWCNT dispersions was evaluated 1 h after preparation by measuring the ζ-potential with a Dynamic Light Scattering (DLS) apparatus, Zetasizer 5000, Malvern Instruments, UK.

2.3. Preparation of Mt/MWCNT hybrid nanofiller

The most stable Mt/MWCNT dispersion (section 2.2) was lyophilized with a Scanvac Coolsafe freeze dryer (Germany), equipped with vacuum pump (2.3/2.8 m^3/h, 4.10^{-4} mbar). The freeze-dried nanofiller, which is Mt/MWCNT hybrid produced by this lyophilization process, is referred to as hybrid and abbreviated as "hyb" throughout the rest of the manuscript.

2.4. Preparation of PLA/hyb nanocomposites

A two-step solution mixing and melt mixing method was adopted for the preparation of PLA/hyb nanocomposites. The first step was the preparation of masterbatch films via solution mixing. The composition of the masterbatch is 1 g of PLA and 0.05, 0.1 and 0.2 g of hyb dispersed by ultrasonication in dichloromethane (50 mL). The dispersion was under

continuous magnetic stirring until most of the solvent evaporated. The resulting slurry was dried under vacuum at 50 °C to obtain the masterbatch film. Thereafter, the dried masterbatch film and PLA were fed into a Haake-Buchler Reomixer (model 600) of 69 cm^3 volumetric capacity, with twin-roller blades, at 180 °C and a speed 30 rpm for 5 min to prepare the nanocomposites, according to the composition given in Table 2. The obtained nanocomposites were molded into specimens, by compression at 180 °C, with a hot-pressing machine (Paul-Otto Weber GmbH, Germany). Additionally, nanocomposite samples were annealed at 120 °C for 1 h to crystallize them.

Table 1

Different amounts of Mt and MWCNT used to determine optimum stable Mt/MWCNT hybrid nanofillers mass ratio

No.	Sample	Montmorillonite (mg)			Carbon nanotubes (mg)	
		Mt Na^+	Mt 10A	Mt 20A	MWCNT	MWCNT-f
1	Mt Na^+	30				
2	Mt 10A		30			
3	Mt 20A			30		
4	CNT				30	
5	CNT-f					30
6	Mt Na^+/MWCNT 1:1	15			15	
7	Mt Na^+/MWCNT 2:1	20			10	
8	Mt Na^+/MWCNT 4:1	24			6	
9	Mt Na^+/MWCNT-f 1:1	15				15
10	Mt Na^+/MWCNT-f 2:1	20				10
11	Mt Na^+/MWCNT-f 4:1	24				6
12	Mt 10A/MWCNT 1:1		15		15	
13	Mt 10A/MWCNT 2:1		20		10	
14	Mt 10A/MWCNT 4:1		24		6	
15	Mt 10A/MWCNT-f 1:1		15			15
16	Mt 10A/MWCNT-f 2:1		20			10
17	Mt 10A/MWCNT-f 4:1		24			6
18	Mt 20A/MWCNT 1:1			15	15	
19	Mt 20A/MWCNT 2:1			20	10	
20	Mt 20A/MWCNT 4:1			24	6	
21	Mt 20A/MWCNT-f 1:1			15		15
22	Mt 20A/MWCNT-f 2:1			20		10
23	Mt 20A/MWCNT-f 4:1			24		6

205

206 **Table 2**

207 Composition of the prepared nanocomposites.

No.	Sample	PLA (%wt)	Mt/MWCNT hybrid (%wt)
1	PLA	100	0
2	PLA0.5hyb	99.5	0.5
3	PLA1.0hyb	99	1
4	PLA2.0hyb	98	2

208 *2.5. Characterizations*

209 X-ray diffraction (XRD) analysis was carried out using a Rigaku MiniFlex II DESKTOP
210 X-ray Diffractometer with Cu Kα radiation ($\lambda = 0.154$ nm). Measurements were performed
211 over the ranges 2 - 10° and 10 - 50°, both with a step of 0.05 º and speed 1 º/min. The clay
212 interlayer distance d was evaluated from the XRD patterns using Bragg's formula given by
213 (Raji et al., 2018):

214 $$2d \sin\theta = n\lambda \quad (1)$$

215 where θ, n and λ represent, diffraction angle, integer of the diffraction band order ($n = 1$)
216 and wavelength of X-ray, respectively.

217 Fourier-transform infrared (FTIR) spectra were obtained using a Perkin-Elmer Spectrum
218 One FT-IR, with a resolution of 4 cm^{-1} and using 16 scans.

219 The dispersion state of Mt/MWCNT hybrid in the PLA was examined by transmission
220 electron microscopy (TEM), using a Jeol JEM 1010 electron microscope operated at 100kV.
221 The TEM specimens were prepared by cutting thin sections of the studied materials with a
222 Leica UCT Ultracut ultramicrotome and collecting them on 400-mesh Au grids.

223 Differential scanning calorimetry (DSC) analyzes were conducted with a Perkin-Elmer
224 Pyris 6 DSC, under 20 mL/min flow of nitrogen (N_2). The experiments were conducted on
225 samples mass of about 8 mg. In order to erase any thermal history, each sample was taken

through heating-cooling cycle twice, first heated from 20 to 190 °C at a rate of 10 °C/min, held for 1 min at 190°C, and then cooled from 190 °C to 20 °C at a rate of 10 °C/min. The crystallinity X_c of the neat PLA and its nanocomposites were calculated using equation (2) (Hu et al., 2017):

$$X_c = \frac{\Delta H_m - \Delta H_{cc}}{\Delta H_m^o \times f} \times 100\% \quad (2)$$

where ΔH_m and ΔH_{cc} are melting and crystallization enthalpies, ΔH_m^o is melting enthalpy for 100% crystalline PLA (93.7J/g), f is the percentage weight of the PLA in the nanocomposite.

Thermogravimetric analyzes (TGA) were performed with a Setaram SETSYS TG-DTA 16/18 instrument. Samples of 3±0.5 mg were placed in alumina crucibles and were measured in dynamic conditions, in the temperature range from 26 to 600 °C, with a heating rate of 20 °C/min, with a 50 mL/min N_2 flow. In addition, TGA under kinetic conditions were performed, with the additional heating rates of 5, 10 and 15 °C/min, using the NETZSCH Kinetics Neo software, version 2.4.6. For this test, samples of the same mass and under the same aforementioned conditions were adopted.

The mechanical tensile tests were achieved using an Instron 3344 dynamometer (USA), according to ASTM D638, at a crosshead speed of 2 mm/min. Average of three dumbbell-shaped samples were tested for each kind of material to determine the mechanical characteristics of the studied neat PLA and nanocomposites.

3. Results and discussion

3.1. Structures of the montmorillonite nanoclays

The Small Angle X-ray diffraction (SAXD) results of the crystallographic structures of Mt Na^+, Mt 10A and Mt 20A are presented in Fig. 2. The unmodified Mt Na^+, that contains primarily Na^+ exchangeable cations recorded $2\theta = 7.59°$ equivalent to 1.163 nm basal *d*-

249 *value*. The result is consistent with literature (Tunç and Duman, 2011; 2010). The modified
250 nanoclays Mt 10A and Mt 20A featured sharp diffraction peaks at lower positions compared
251 to unmodified Mt Na^+, i.e. at $2\theta = 4.6°$ and $2\theta = 3.5°$, corresponding respectively to the
252 interlayer distances $d = 1.918$ nm and $d = 2.521$ nm. This suggests that the quaternary
253 ammonium ions intercalated into the modified clays Mt 10A and Mt 20A layers resulted in
254 the expansion of basal spacing (Qin et al., 2018). However, the diffractograms of Mt 20A
255 shows additional smaller peak around 7.07° ($d = 1.249$ nm) which is not attributed to d_{002}
256 but close to crystallographic *d-value* of Mt Na^+ ($d = 1.163$ nm). This implies that Mt 20A
257 contains some amount of tactoids that have nanoclays platelets intercalated with Na^+ cations
258 (Timochenco et al., 2010). This second peak, at 7.07°, also suggests an insignificant edge
259 grafting or interlayer of 2MHT ammonium molecules within the Mt 20A layers (Raji et al.,
260 2018). Moreover, by comparing the intensities and shapes of Mt 10A and Mt 20A, it can be
261 agreed that Mt 10A presented the more disordered layer-structure while the very sharp and
262 high peak of Mt 20A shows higher ordered layer-structure (Zhuang et al., 2015; Qin et al.,
263 2018). Thus, from the above, we can conclude that the disordered layer-structure in Mt 10A
264 is probably an advantage, over other clays, for easier intercalation of other phases.

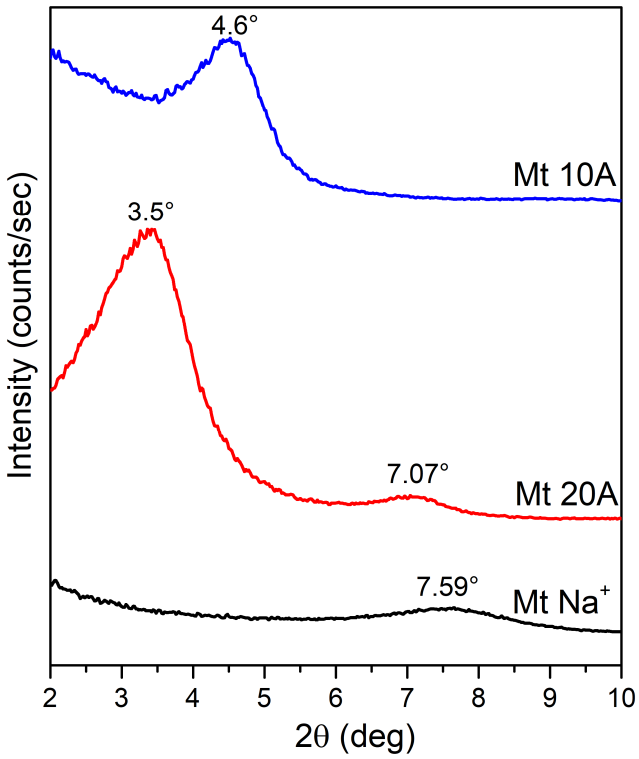

Fig. 2. Small angle X-ray diffractograms of Mt Na^+, Mt 20A and Mt 10A.

3.2. Evaluation of dispersion quality of the nanoparticles in water

The sedimentation photographs of different Mts, MWCNTs and combinations of Mt/MWCNT hybrid suspensions are shown in Figs. 3 and 4; after 1 h, 24 h and 1 week of suspension. Single dispersion of Mt Na^+ or Mt 10A in aqueous solution by agitation showed significant level of the nanoclays stability in the aqueous solution up to 24 h, thereafter, sediments begun to grow at the bottom of the vial with time (Fig. 3). In contrary, for Mt 20A suspension, significant amount of sediments was obtained after 1 h, at the bottom of the vial, leaving almost clear solution at the top. Pristine Mt Na^+ is greatly hydrophilic because of the rich Na^+ cations in the clays, which are easily hydrated, and that makes it disperses fine in water on agitation (Narro-Céspedes et al., 2018). Likewise, the modifying agent 2MBHT on Mt 10A was suspected to provide good interaction with water molecules that promoted the nanoclay suspension in the solution. Ha (2006) reported that the replacement of an hydrogenated tallow group with a benzyl group gives Mt 10A a moderate hydrophobicity as

well as compatibility with poly(butylene terephthalate). However, Mt 20A is modified with only hydrogenated tallow group. After 1 h of the solution preparation, singly prepared pristine MWCNT or MWCNT-f suspension settled towards the bottom of the of vial leaving few MWCNT suspension at the top (Fig. 3), and the sediment increased rapidly with time. This is attributed to the inherent high force of attraction between the MWCNT nanoparticles.

With varying ratio of Mt Na^+ over MWCNT (Fig. 4a), the dispersions remained black solution beyond 1 h. However, after 24 h, sediments began to build-up leaving dark but a bit transparent solution at the top of the vial and this progressed with time. The samples with Mt Na^+/MWCNT-f (Fig. 4b) maintain black aqueous solution until 24 h, when the solution turned transparent-brownish with black sediments after 1 week. The fair maintenance of dark solution before the clear separation shows little level of stability, that is, weak promotion of MWCNT suspension and dispersion in water as result of Mt Na^+ incorporation.

On addition of Mt 10A with MWCNT (Fig. 4c) or MWCNT-f (Fig. 4d), the entire sample ratios showed high level of stable black aqueous solutions beyond 24 h, with insignificant sedimentation after a week. This suggests that Mt 10A greatly support the dispersion of both pristine and functionalized MWCNT, independently of the standing period and irrespective of the nanofillers ratio, when compared with Mt Na^+.

As seen in Fig. 4e and 4f, the presence of Mt 20A did not keep either the MWCNT or MWCNT-f particles suspended in the solution. The consistent inability of Mt 20A to influence MWCNT suspension in the aqueous solution suggests that the 2MHT ion over Mt 20A does not interact with neither of the MWCNTs nor the aqueous medium. As earlier identified in the SAXD pattern of Mt 20A, insignificant edge grafting or interlayer of 2MHT ammonium molecules within the Mt 20A layers, may have prevented the MWCNT intercalation into the clay platelets. Thus, the two nanoparticles discretely settled rapidly.

Conclusively, absence of clay in any of the vials brings about complete sedimentation of MWCNT owing to strong van dal Waal forces between the MWCNT particles and deficient chemical affinity with the aqueous medium (Lee et al., 2007; Wang et al., 2009). Garcia et al. (2015) remarked that chemical modification of phyllosilicate Mt raises its hydrophobicity, and Mt 20A is more than Mt 10A. The 2MHT ammonium cation of Mt 20A has a high density and hydrophobicity because of its tallow chains (Galimberti et al., 2015), hence, its rapid sedimentation in solution and the least compatibility with MWCNT. Re-aggregation of dispersed MWCNT, due to van der Waals force resulting from high surface energy, seemed to be mostly prevented by the platelets of Mt 10A nanoclay type. This presents Mt 10A to be of higher compatibility with either of the two carbon nanotubes.

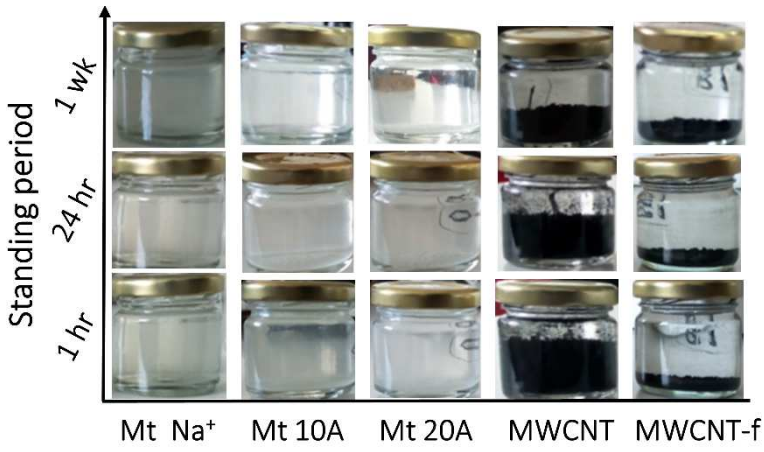

Fig. 3. Sedimentation of Mt Na^+, Mt 10A, Mt 20A, MWCNT and MWCNT-f at different periods.

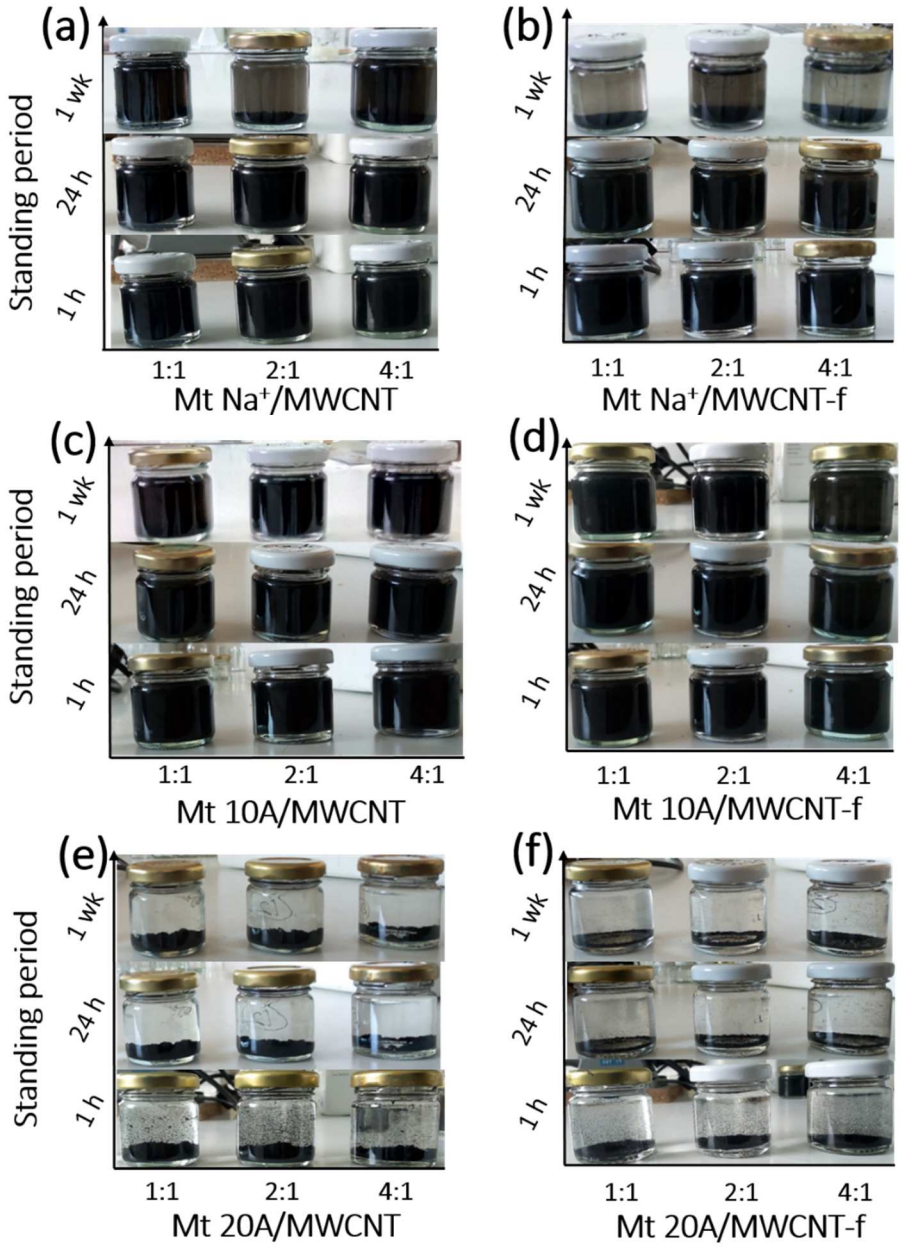

Fig. 4. Sedimentation of different ratios of (a) Mt Na^+/MWCNT; (b) Mt Na^+/MWCNT-f; (c) Mt 10A/MWCNT; (d) Mt 10A/MWCNT-f; (e) Mt 20A/MWCNT; (f) Mt 20A/MWCNT-f at different standing periods.

ζ-potential can evaluate the synergetic interactions between two different nanofillers (Galimberti et al., 2015). The dividing line between stable and unstable suspensions is generally taken at either 30 mV or -30 mV. Particles having the zeta potentials higher than +30 mV or lower than -30 mV is normally considered as stable particles (Duman and Tunç, 2009). Nanoparticles with ζ-potential more than +30 mV are regarded as strongly cationic (or

326 less than -30 mV as strongly anionic) (Abouelhag et al., 2017), that is, the particles are stable
327 on dispersion in solution. Fig. 5 presents the plots of the ζ-potential values for the various
328 hybrids of nanoclays and carbon nanotubes, measured with DLS. The ζ-potentials of single
329 MWCNT or MWCNT-f is approximately -13 mV that indicates poor stability. This is in
330 conformity with the results found in sedimentation experiment, and agrees with the
331 bibliography (Chu et al., 2012). Single Mt 20A solution recorded -4 mV. In combination with
332 any of the MWCNTs, absolute ζ-potential values of Mt 20A/MWCNT hybrid nanofillers
333 were ~14 mV, suggesting high tendency of aggregation, as observed in the sedimentation
334 results.

335 Meanwhile, the ζ-potential values of Mt 10/MWCNT or Mt 10/MWCNT-f were greater
336 than those of Mt Na^+/MWCNT or Mt Na^+/MWCNT-f, with highest value of about 46 mV,
337 observed for the ratio 2:1. This supposes good stability or low tendency of the particles to
338 aggregate (Jain, 2012; Ma et al., 2019). Consequently, Mt 10A and MWCNT with a mass
339 ratio 2:1 were selected for the preparation of the Mt/MWCNT nanohybrid particles. Pristine
340 MWCNT was chosen over functionalized MWCNT for economic and environmental reasons,
341 as well as the sustenance of carbon nanotube structural integrity, which may be affected by
342 functionalization (Guadagno et al., 2011; Vennerberg et al., 2014; Alshammari and
343 Wilkinson, 2016).
344

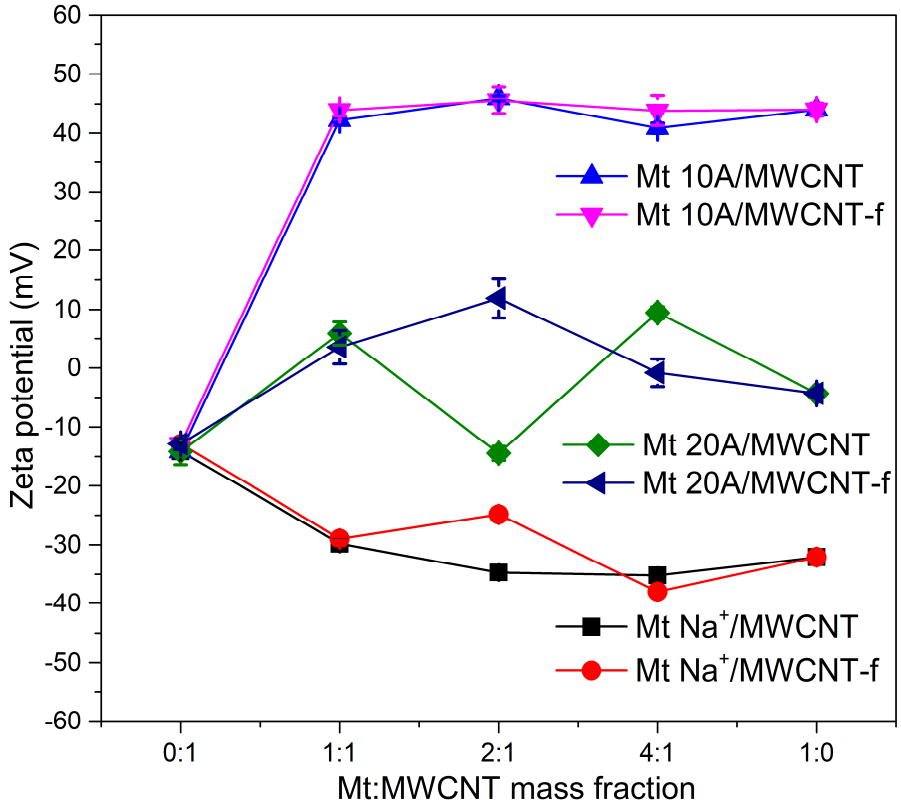

Fig. 5. Zeta potential values against Mt/MWCNT hybrid mass fraction ratio.

3.3. Structural characterization of the Mt/MWCNT hybrid

The prepared Mt/MWCNT hybrid was characterized by XRD and FTIR, which are presented in Fig.6 and Fig.7, respectively. The XRD peak of Mt became broader and shifted from $2\theta = 4.6°$ (Mt 10A; $d_{100} = 1.918$ nm) to 4.4° (hyb; $d_{100} = 2.006$ nm) after its hybridization with MWCNT. The shift in the diffraction peak position is caused by the increase in the basal spacing in the clays from 1.918 nm in Mt 10A to 2.006 nm in hyb. This suggests intercalation of MWCNT in the clay platelets, which could prevent the re-aggregation of MWCNT, as the nanoclays do prevent the formation of van da Waal forces between the nanotubes (Zhuang et al., 2015; Qin et al., 2018). The diffraction peak of MWCNT at 26 ° corresponds to the (002) plane of graphitized multi-walled carbon nanotubes (Gorrasi et al., 2013; Mumtazah et al., 2019), and it is present in the Mt/MWCNT hybrid at the same angle. Similarly, the diffraction peaks of Mt at 20° and 35° correspond to

montmorillonite (110) and (105) planes (Manikandan et al., 2012; Galimberti et al., 2015) and these two peaks are also present in the prepared hybrid but with lower intensities, suggesting improved exfoliation of Mt 10 platelets (Manikandan et al., 2012; Raji et al., 2016). Hence, the SAXD and WAXD studies on Mt/MWCNT hybrid shows adequate interactions occurred between the MWCNT and Mt nanoparticles that resulted in an intercalated structure. Furthermore, two new characteristic peaks at 45.4° and 31.6° are identified. The peak at 45.4° corresponds to the (100) reflection of graphite, along with the (002) plane at 26°, which is believed to arise from high quality multi-walled MWCNTs (Zhu et al., 2004; Wu et al., 2019). The peak at 31.6° is likely to be impurity of iron catalyst on MWCNT during its synthesis (Hapuarachchi and Peijs, 2010; Norazlina et al., 2019). Finally, since there are no shifts in the peak positions of both Mt 10A and MWCNT, it can be implied that their structures were preserved (Kumar et al., 2018).

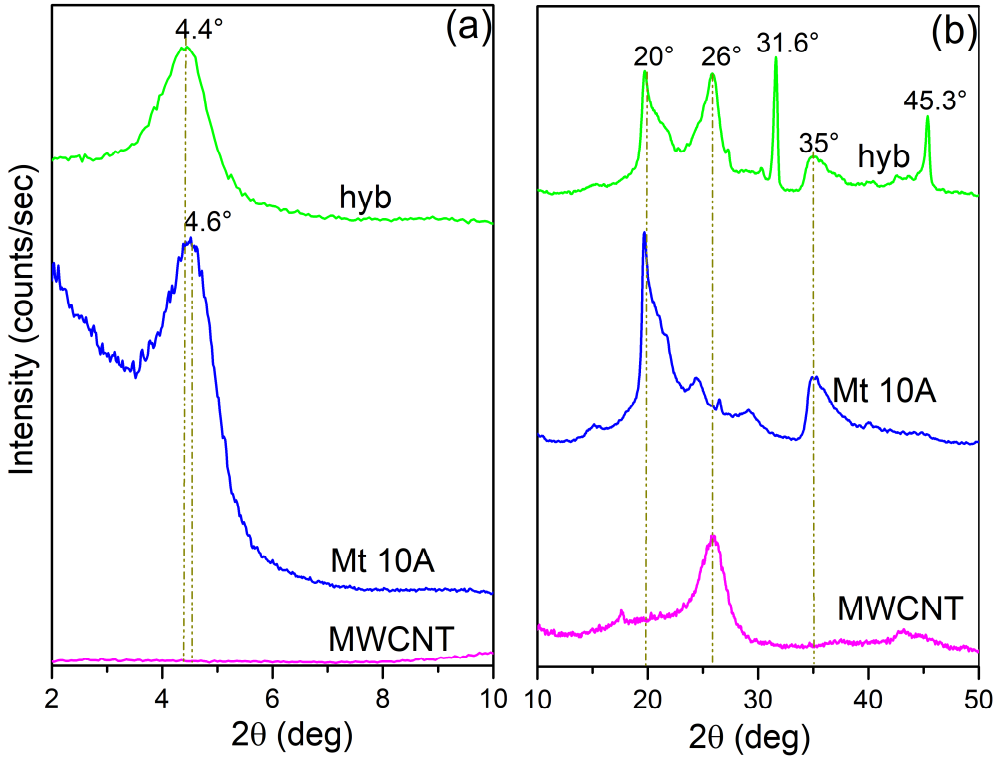

Fig. 6. (a) SAXD and (b) WAXD of MWCNT, Mt 10A and the lyophilized Mt 10A/MWCNT hybrid nanofillers.

374 The FTIR spectra of the nanofillers are presented in Fig. 7. For Mt 10A, the absorption
375 band at 3631 cm^{-1} represents the -OH stretching of Si-OH and Al-OH (Shabanian et al.,
376 2016). The band at 1046 cm^{-1} is ascribed to Si-O-Si stretching vibration of Mt (Pan et al.,
377 2014). The two peaks at 516 and 462 cm^{-1} correspond to stretching vibration of the Al-O and
378 bending vibration of Si-O in Mt, respectively (Zhang et al., 2003; Arjmandi et al., 2014;
379 Arjmandi et al., 2015b). The strong bands of MWCNT at 3465 cm^{-1} indicates isolated surface
380 stretching vibrations of -OH group and/or carboxyl group (Montanheiro et al., 2015), while
381 1636 cm^{-1} is assigned to aromatic ring stretching, of the backbone of MWCNT, that indicates
382 the presence of graphitic structure (Zhou et al., 2018). The hybrid filler (hyb) shows all the
383 peaks of Mt 10A at the same wavenumbers, but the main peaks of MWCNT are absent. This
384 could be partially related to the greater amount of Mt 10A (Mt/CNT 2:1 mass ratio) in the
385 hybrid formulation (Santangelo et al., 2011). Besides, as concluded from XRD, MWCNT
386 intercalated between the clay platelets, which might limit its detection by FTIR.

387

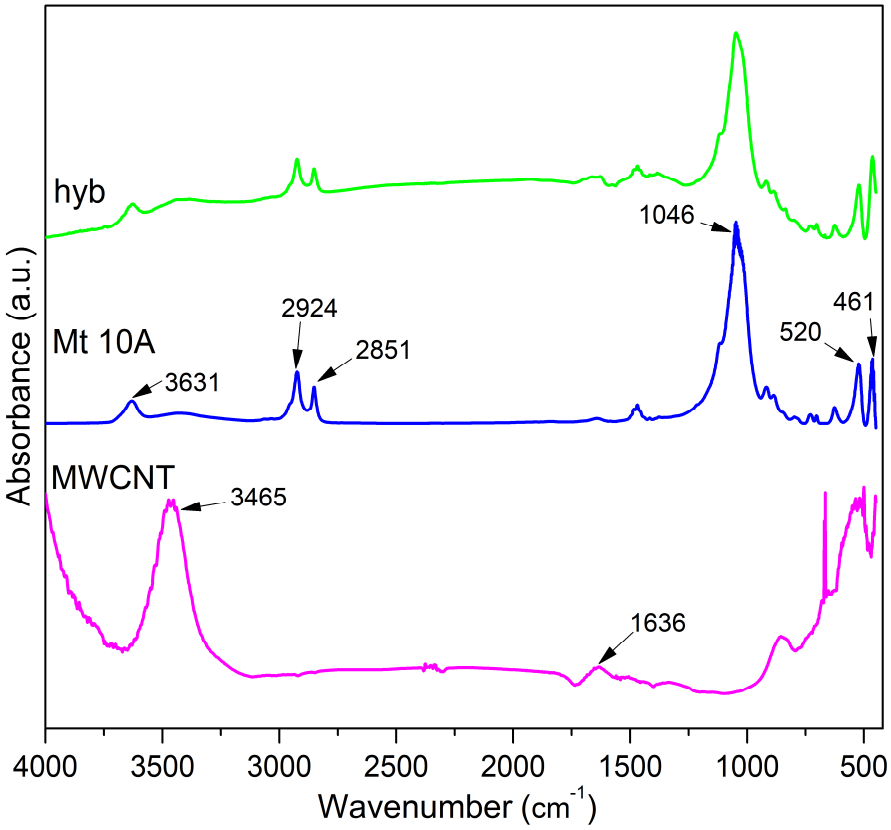

Fig. 7. FTIR spectra of MWCNT, Mt 10A and their hybrid (hyb).

3.4. Structural and morphological characterizations of PLA/hyb nanocomposites

The XRD diffractograms of PLA/hyb nanocomposites are presented in Fig. 8. The diffraction peak related to the nanoclay ($2\theta = 4.4°$) in the Mt /MWCNT hybrid disappeared in the diffractogram of PLA/hyb nanocomposites (Fig. 8a), which suggests the exfoliation of the Mt layered silicate in the polymer matrix (Gorrasi et al., 2013; Shabanian et al., 2016). From the diffractograms of Fig. 8b, PLA/hyb nanocomposites displayed no other peaks aside the PLA amorphous halo, which implies good dispersion of hyb in the nanocomposites. Therefore, one could conclude that there is a synergy, between the nanoclay and MWCNT particles, that helps in the exfoliation of clay platelets. This observed structure in the PLA/hyb nanocomposite supports the discussed intercalation of Mt by the MWCNT in the prepared Mt/MWCNT hybrid particles (section 3.3), which now translate to almost complete exfoliation of the nanoclay platelets within the PLA matrix (Fig. 8a). Similarly, no obvious

peak of graphitic carbon is detected (Fig. 8b), substantiating the hypothesis that the even dispersion of clay in Mt/MWCNT hybrid is sustained, and as such prevents any re-agglomeration of MWCNT particles due to van da Waal attraction forces in the PLA matrix. This PLA-hyb interaction is assumed to translate into improved properties in the ternary bulk nanocomposites. After annealing, the three peaks (17.87°, 20.25° and 23.44°) emerge on the diffractogram of PLA (Fig. 8c) and correspond to the orthorhombic crystalline α-PLA form (Jia et al., 2019). They are all retained in the diffractograms of the nanocomposites, which implies that the crystalline structure of PLA is not altered by the incorporation of lyophilized Mt/MWCNT hybrid nanofillers (Barrau et al., 2011).

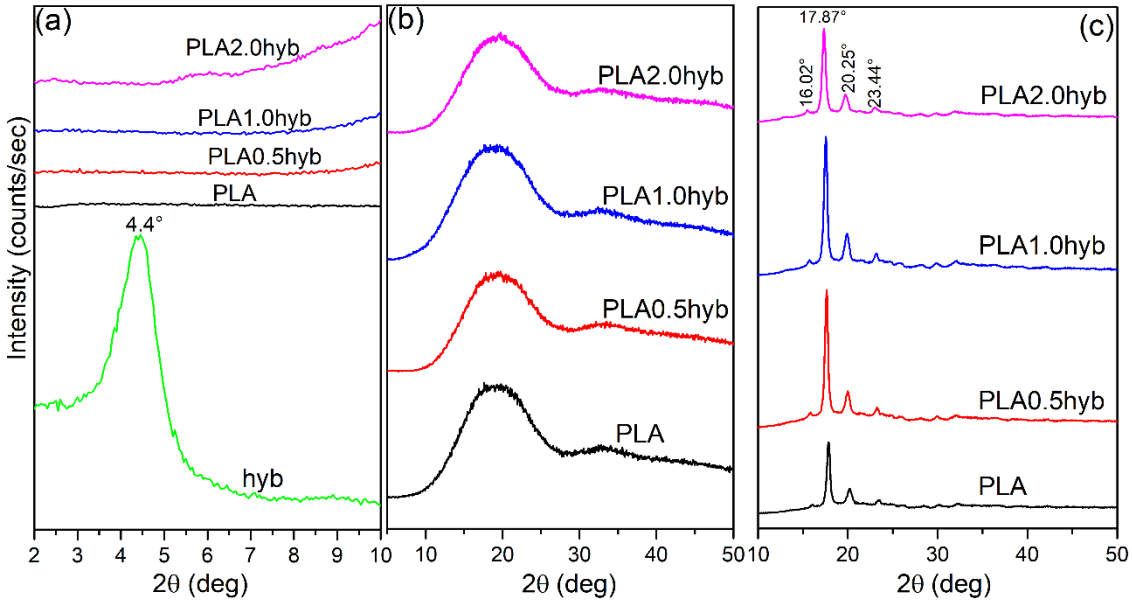

Fig. 8. XRD diffractograms of neat PLA and PLA/hyb nanocomposites (a) in small angles, (b) wide angles, (c) annealed PLA and PLA nanocomposites at 120 °C for 1 h.

Fig. 9 (a-f) represent the TEM images of PLA0.5hyb (a and b), PLA1.0hyb (c and d) and PLA2.0hyb (e and f). These images reveal that MWCNT and Mt particles are homogenously dispersed in all the samples, which corroborate the XRD analyzes, and agree with the findings of Bai et al. (2020) and Ma et al. (2007). This result suggests that the hybridization of Mt and CNT promotes the dispersion of the nanoparticles and prevents CNT aggregation.

From Fig. 9 (a, c and e), the densification of the particle distribution is observed with the increase of the fillers concentration. The arrows in Fig. 9 (a, c and e) indicate individual dispersed MWCNT. Fig. 9 (b, d and f) highlights single carbon nanotubes in connection with exfoliated Mt platelets, which depicts that each of the two nanofillers influences the dispersibility of the other, i.e. synergetic interactions seem to occur between the two different nanofillers. Finally, from the TEM results presented above, one may conclude that the lyophilization treatment and the nanocomposites preparation process have positive effect on the distribution of the hybrid nanoparticles in PLA matrix.

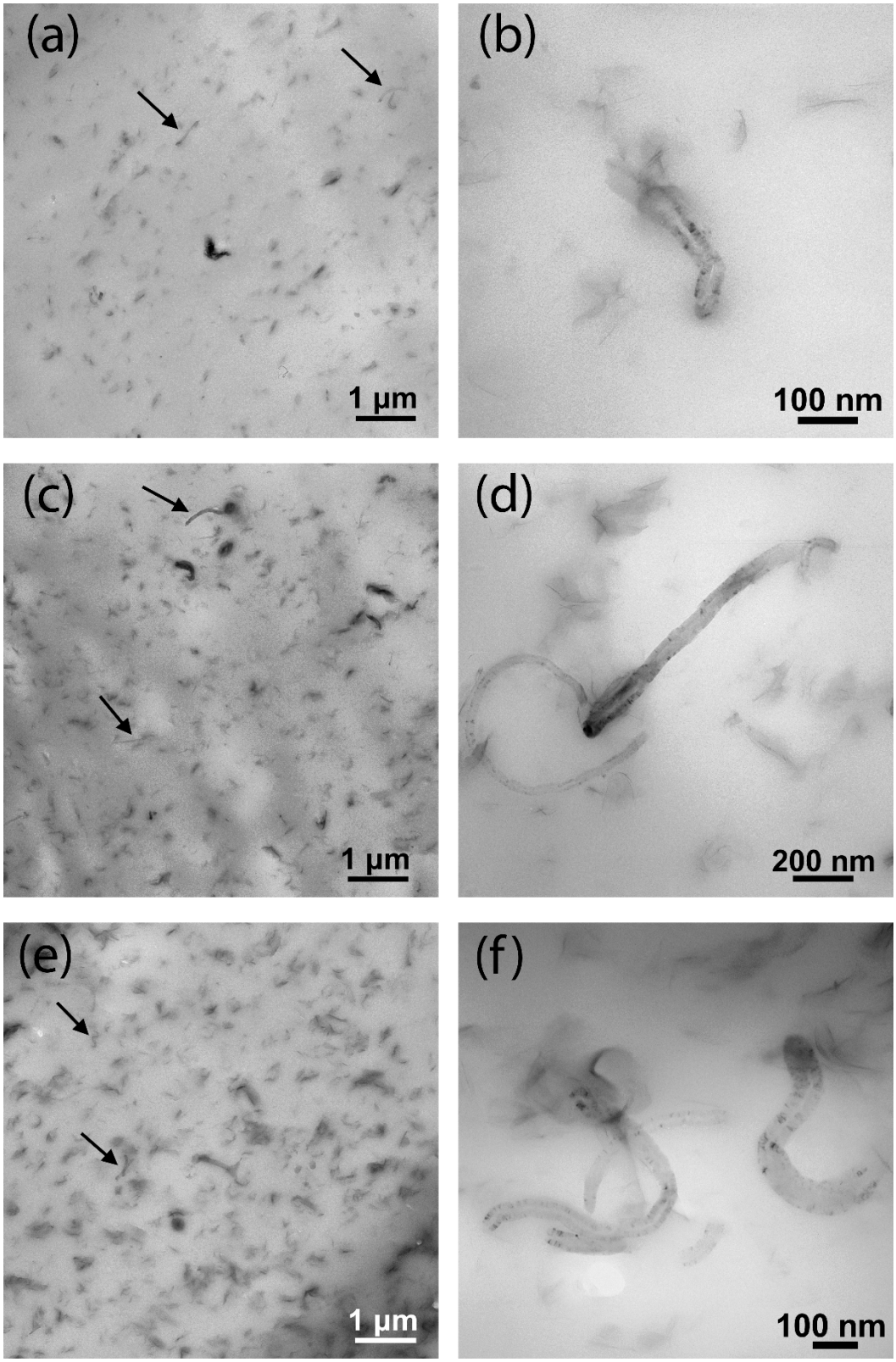

427

428 **Fig. 9.** TEM images of PLA0.5hyb (a and b), PLA1.0hyb (c and d) and PLA2.0hyb (e and f).

429

In the FTIR spectrum of neat PLA (Fig. 10), the peaks at 3657 and 3507 cm^{-1} correspond to –OH stretching vibrations (Arjmandi et al., 2014; Shabanian et al., 2016). Both peaks at 2994 and 2943 cm^{-1} are attributed to the aliphatic asymmetric stretching vibration of the –CH moiety (Arjmandi et al., 2015a; Shabanian et al., 2016). The carbonyl (C=O) group stretching vibration appears at 1757 cm^{-1} as a sharp peak (Fu et al., 2018; Huang et al., 2020). The characteristics bands at 1454 and 1047 cm^{-1} are the bending groups of $–CH_3$ and –OH, respectively, while 1361 cm^{-1} represents the bending vibrations of $–CH_2$ (Choksi and Desai, 2017; Fu et al., 2018). The band at 1097 cm^{-1} corresponds to the C-O stretching vibration (Arjmandi et al., 2015a; Hu et al., 2017). The C-C stretching vibrations are reflected at 954 and 865 cm^{-1} (Arjmandi et al., 2014; Y. Liu et al., 2019).

It is obvious from Fig. 10 that all characteristics peaks of PLA are also in the spectra of the PLA/hyb nanocomposites. In addition, the spectra of the PLA/hyb nanocomposites show two new weak peaks at 516 and 462 cm^{-1} that represent the stretching vibrations of Al-O and bending vibrations of Si-O from the nanohybrid (Zhang et al., 2003; Arjmandi et al., 2014; Arjmandi et al., 2015b), perhaps owing to the larger amount of Mt in the hybrid nanofillers (i.e., Mt:MWCNT 2:1). The weak intensity of the Si-O peak suggests high degree exfoliation of the nanoclay (Molinaro et al., 2013), as also implied by the XRD results. Mt has a high number of uniformly distributed polar sites along its structure, which support hydrogen bonding with PLA (Arjmandi et al., 2015b). However, because of the low mass fraction of the Mt/MWCNT hybrid nanofillers in the nanocomposite, the detection of other features from interacting moieties may be difficult (Terzopoulou et al., 2016).

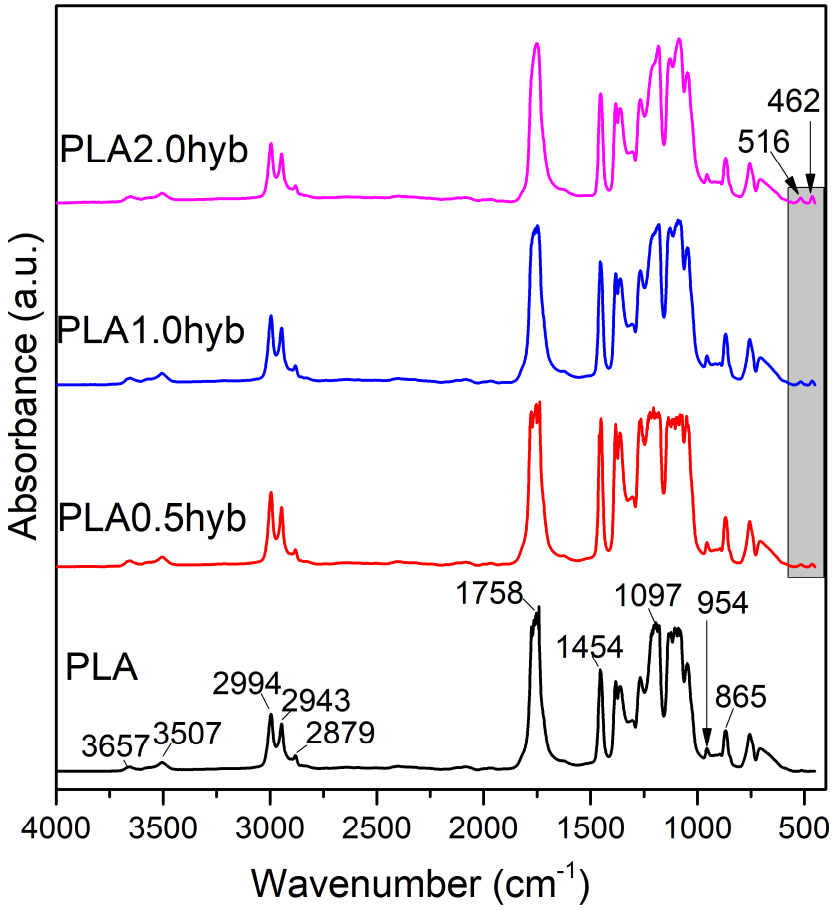

Fig. 10. FTIR spectra of neat PLA and PLA nanocomposites.

3.5. Thermal properties of PLA/hyb nanocomposites

The DSC second heating thermograms of the PLA and its nanocomposites, shown in Fig. 11, were used for the thermal analysis, as the first scan was to reduce thermal history. The glass transition temperature (T_g), cold crystallization temperature (T_{cc}) and melting temperature (T_m), crystallization enthalpy (ΔH_{cc}), melting enthalpy (ΔH_m) and crystallinity (X_c) were obtained and summarized in Table 3. For neat PLA, T_g was identified at 63.6 °C. The exothermic peak corresponding to T_{cc} appeared at 119.6 °C, while the endothermic peak at 149.9 °C represents the PLA melting point. The results are in accord with those found in literature (Choksi and Desai, 2017; Terzopoulou et al., 2019a; Pires et al., 2020). The T_g of the nanocomposites are approximately unchanged, while T_m of these nanocomposites slightly increased compared to the neat PLA. Chattopadhyay et al. (2009) reported similar little

change in T_g and related it to the possibility of more prominent filler-filler interaction than the polymer-filler interaction. The bimodal T_g peaks recorded on PLA2.0hyb can be related to several factors such as crystal structures, processing conditions (Pires et al., 2020). The observed minor changes in T_m may be traced to perturbation of the PLA stereoregularity that is defined by enthalpy or entropy of the isomer units causing the PLA crystal structure to show minute melting temperature changes (Molinaro et al., 2013). The slight increase in melting temperature can also be attributed to the rearrangement of polymer chain that becomes more effective owing to the nanofillers high surface energy (Vukić et al., 2019).

The PLA/hyb nanocomposites show significant increase in the crystallization temperature compared to neat PLA; determined in the range of 124 - 128 °C. The observed significant increase of the crystallization temperature for all the nanocomposites supports that there is a strong interaction between the PLA matrix and the incorporated lyophilized nanohybrid (Sibeko, 2012). Furthermore, the obvious increase in the nanocomposites T_{cc} compared to neat PLA (119.57°C) connotes that the PLA-hyb interaction restricted the PLA molecular motion (Hu et al., 2017). Notably, the nanocomposite with the least filler loading (PLA0.5hyb; 0.5 %wt Mt/MWCNT) shows the most significant T_{cc} and T_m increase. Except for PLA0.5hyb with reduced X_c, it was found that crystallinity grows with the hyb concentration significantly (Table 3). The observed crystallinity reduction at lower concentration may be associated with the crystal growth limitation as well as imperfect crystal structure (Shayan et al., 2019). In other words, the initial X_c depression may be due to two competing effects of hyb in restricting PLA chain motion and its nucleating effect that promoted the crystallization kinetics of the matrix (Sanusi et al., 2020b)(Hu et al., 2017). Meanwhile, the subsequent crystallinity improvement can be due to uniform dispersion revealed by the TEM images, and increased active nucleation sites generated by the Mt/MWCNT hybrid (Chu et al., 2012). Mt (Jia et al., 2019) and MWCNT (Vukić et al.,

2019) are revealed sometimes to be a nucleating agent, so their incorporation as components of Mt/MWCNT is suspected to play a synergistic role of improving X_c in PLA. Hence, it can be inferred that the lyophilized Mt/MWCNT hybrid increased the amount of crystallinity in the matrix, and thus reinforced the matrix.

Table 3

Thermal properties of PLA and PLA/hyb nanocomposites.

Sample	T_g (°C)	T_{cc} (°C)	ΔH_{cc} (J/g)	T_m (°C)	ΔH_m (J/g)	X_c
PLA	63.60	119.57	20.44	149.94	21.21	44.78
PLA0.5hyb	64.10	128.19	14.54	151.93	14.79	33.19
PLA1.0hyb	63.22	124.73	27.61	150.79	19.83	56.67
PLA2.0hyb	63.60	126.22	29.37	151.12	17.22	62.61

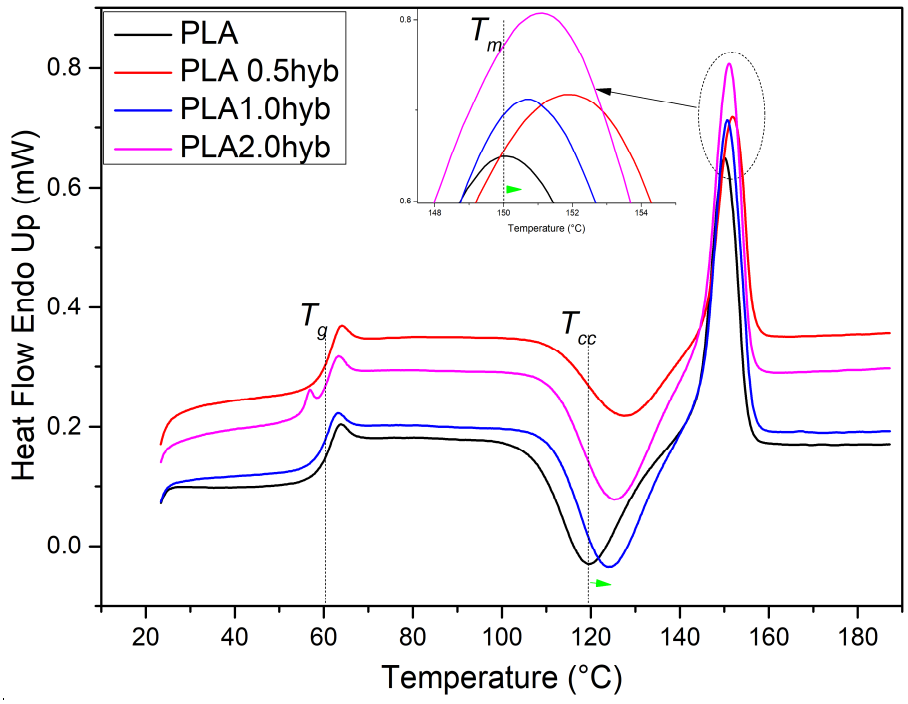

Fig. 11. DSC thermograms of PLA and nanocomposites obtained during second heating cycle at 10 °C/min.

3.6. Thermal stability

Thermal stability of polymer is critical, as the property is considered as the limiting factor for processing as well as for end-use applications (Terzopoulou et al., 2019b). Fig. 12 shows

501 the TGA thermograms of the PLA and its nanocomposites; while Table 4 presents the
502 summary of the thermal performance i.e., the initial, 10% mass loss, maximum mass loss and
503 final degradation temperatures as T_{onset}, $T_{d,10\%}$, T_p and T_{comp}, respectively. The PLA/hyb
504 nanocomposite reinforced with lyophilized Mt/MWCNT particles gained improved thermal
505 stability properties at the least nanofillers concentration of 0.5 wt% (PLA0.5hyb), as shown
506 in Table 4 and Fig. 12. Beyond this loading, the thermal stability of the PLA/hyb
507 nanocomposites fall, samples PLA1.0hyb and PLA2.0hyb almost have similar decrease in the
508 characteristics degradation temperatures. Malkappa et al. (2018) reported that promotion of
509 PLA degradation, due to reduced $T_{d,10\%}$ at lower temperature, forms thermally insulating
510 char quicker and prevents further degradation of polymer. Another explanation can be the
511 attainment of percolation threshold point at 0.5 %wt loading of the Mt/MWCNT (hyb) in the
512 PLA matrix. Thus, at higher loading, the 3D percolation structure seems to be well
513 established thereby creating a physical network of interaction with the volatile component
514 and conduction of heat that results in promotion of decomposition process (Chu et al., 2012;
515 Pandey et al., 2014; Shayan et al., 2019). Similarly, the TEM images (section 3.4) support the
516 fact that there are interactions between Mt and MWCNT nanoparticles, which are
517 homogenously distributed in PLA and could lead to the formation of 3D network of the
518 Mt/MWCNT hybrid in the matrix.

519 Influence of heating rate is another vital factor that affects thermal degradation process,
520 for instance, the conversion and thermal distribution (Lv et al., 2019). In Fig. 13, the mass
521 loss thermograms of the neat PLA and PLA1.0hyb are shown, for four different heating rates
522 of 5, 10, 15 and 20 °C/min. It is clear that the mass loss curves of the samples degradation
523 properties similarly shift towards higher temperature regions with the heating rate increment.
524 This can be due to the heat flow rate variations inside the studied samples (Lv et al., 2019);
525 and thermal lag (i.e. temperature gradient) across the materials sections as a result of the

different heating rates (Mishra and Mohanty, 2018). At lower heating rate, temperature profile in the sample cross-section is presumed to be linear because the inner and outer cores of the material achieve the same temperature at a given time as there exists enough time for heating; while higher heating rate generates reduced heat distribution and poorer heat transfer efficiency (Niu et al., 2017; Lv et al., 2019).

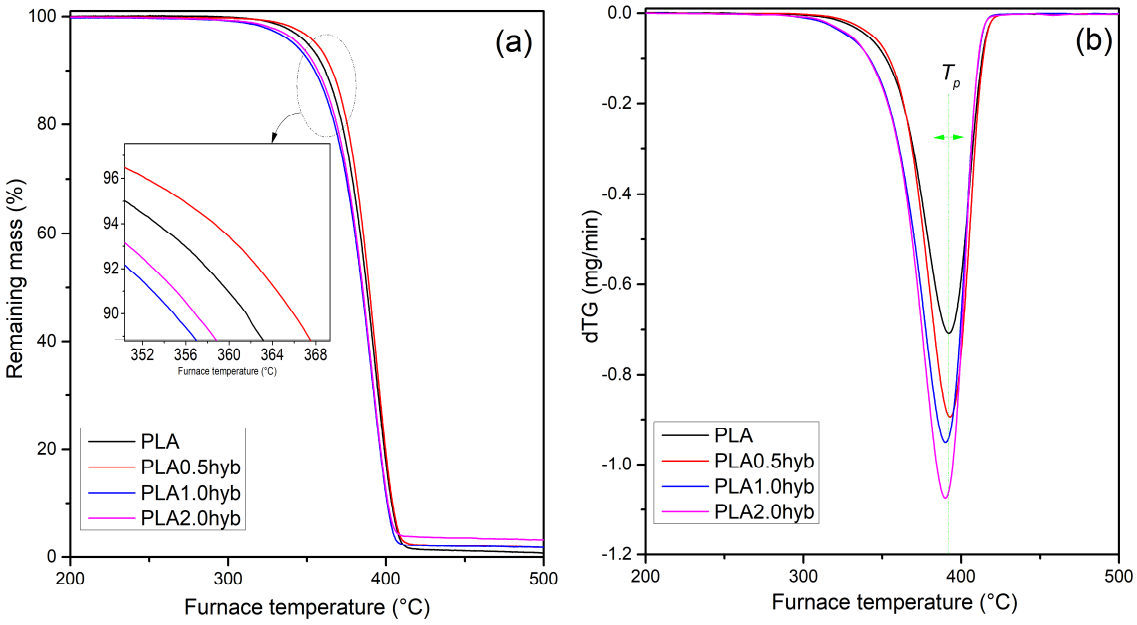

Fig. 12. (a) TGA thermograms; (b) dTG curves.

Table 4

Characteristics thermal degradation temperatures of PLA and its nanocomposites.

Sample	T_{onset} (ºC)	$T_{d,10\%}$ (ºC)	T_{comp} (ºC)	T_p (ºC)
PLA	368.3	361.5	406.4	392.4
PLA0.5hyb	371.7	365.8	406.2	393.0
PLA1.0hyb	363.0	354.8	405.5	390.0
PLA2.0hyb	363.0	356.8	405.5	390.0

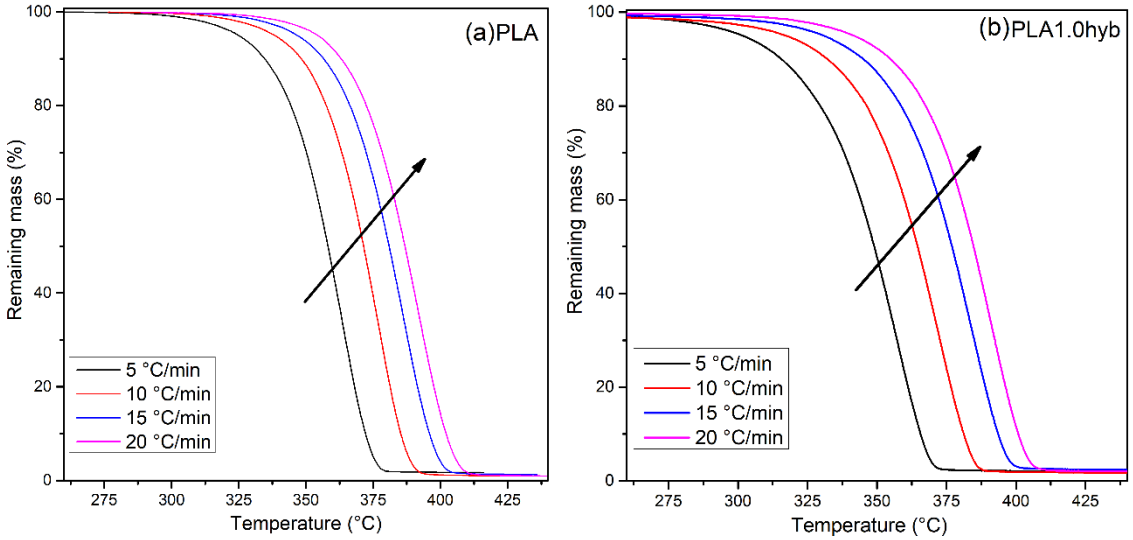

Fig. 13. Mass loss curves of (a) PLA; (b) PLA1.0hyb for four different heating rates of 5, 10, 15 and 20 °C/min. The arrow indicates the increase of heating rate.

3.7. Mechanical properties

The Young's modulus, ultimate tensile strength and deformation at break of PLA and the PLA/hyb nanocomposites were evaluated and summarized in Fig. 14. The elastic modulus of PLA0.5hyb, PLA1.0hyb and PLA2.0hyb are 1.76, 2.0 and 1.65 GPa, respectively, compared to 1.52 GPa in neat PLA. The modulus enhancement in all the nanocomposite samples can be attributed to the reinforcing effect of Mt/MWCNT and stress transfer mechanism from the matrix to the dispersed hybrid nanoparticles (Chiu, 2017; Arjmandi et al., 2015a). The slight reduction of modulus at 2.0 wt% Mt/MWCNT may be due to self-aggregation of hybrid nanoparticles (Zhou et al., 2018), as the percolation threshold was reached earlier at 1.0 wt% (maximum modulus).

The tensile strength increased from 35.5 MPa for PLA to 43.8 MPa for nanocomposite reinforced with 0.5 wt% of Mt/MWCNT, and the values slightly reduced at higher concentrations. The results are in consonant with literature (Zhou et al., 2018; Arjmandi et al., 2015a). It also signified that the Mt/MWCNT particles reduced the mobility of PLA chains (Keshavarzi et al., 2019). The deformation at break also recorded its peak value at 0.5

wt% of Mt/MWCNT, followed by the property reduction at higher concentrations of Mt/MWCNT. Both ultimate tensile strength and deformation at break indicate 0.5 wt% Mt/MWCNT as the percolation threshold which agrees with the value indicated by the DSC and TGA results.

Summarily, since the Young's modulus indicates 1.0 wt% as percolation threshold point, while other material properties (DSC, TGA, strength and deformation at break) suggest it to be at 0.5 wt%, one can conclude that the percolation threshold should be really found between 0.5 and 1.0 wt% Mt/MWCNT.

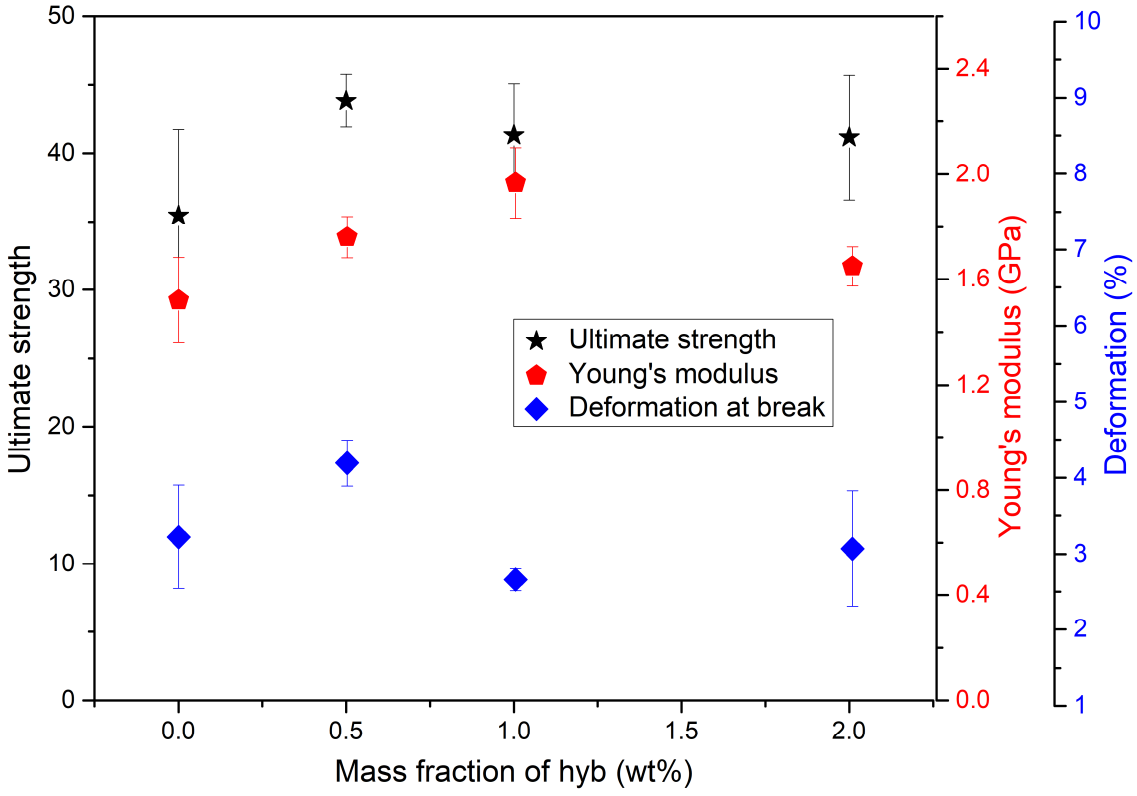

Fig. 14. Mechanical properties of PLA and PLA/hyb nanocomposites.

4. Conclusion

Hybrid of montmorillonite (Mt) and multi-walled carbon nanotubes (MWCNT) was successfully prepared by adopting lyophilization method. The most stable Mt/MWCNT formulation was identified from varying combinations of different types of Mt and MWCNT,

in addition to finding the optimum Mt-MWCNT concentration ratio. Through the XRD and FTIR characterizations, the hybrid was determined to have been successfully prepared with improved nanoclay exfoliation and dispersed MWCNT, while the lyophilization approach was simple and "green". Thereafter, the synthesized Mt/MWCNT hybrid filler was incorporated in poly(lactic acid) (PLA) to study its influence in improving the polymer matrix properties. The nanocomposites prepared by a two-step approach (solution and melt mixing) were fully characterized by XRD, FTIR, TEM, DSC, TGA and mechanical techniques. The physicochemical studies revealed structural interaction between the Mt/MWCNT hybrid and polymer without altering the PLA structure. Moreover, the incorporation of the lyophilized Mt/MWCNT nanoparticles in PLA led to the augmentation in the crystallinity, crystallization and melting temperatures, and mechanical properties of the nanocomposites beyond the neat PLA. This indicates the suitability of the lyophilized Mt/MWCNT hybrid as a nanomaterial for reinforcing polymer matrices. The improvement in material properties is related to homogeneous dispersion of Mt/MWCNT hybrid nanoparticles in the PLA matrix. This homogeneous distribution was confirmed by TEM analysis and partially attributed to the synergy between nanoclay particles and carbon nanotubes. Finally, at low loading of Mt/MWCNT, PLA0.5hyb nanocomposite, the thermal degradation performance was enhanced, while higher concentration of the nanohybrid suggests a well-established percolation network in the nanocomposite, which might serve as a good thermal conductive material.

Acknowledgements

Petroleum Technology Development Fund (PTDF) is acknowledged for the doctoral scholarship grant (Grant Number: 18GFC/PHD/065).

References

593 Abouelhag, H.A., Sivakumar, S.M., Bagul, U.S., Eltyep, E.M., Safhi, M.M., 2017.
594 Preparation and physical characterization of cisplatin chitosan nanoparticles by zeta
595 nanosizer “prime step for formulation and development.” Int. J. Pharm. Sci. Res. 8,
596 4245–4249. https://doi.org/10.13040/IJPSR.0975-8232.8(10).4245-49
597 Al-Saleh, M.H., 2017. Clay/carbon nanotube hybrid mixture to reduce the electrical
598 percolation threshold of polymer nanocomposites. Compos. Sci. Technol. 149, 34–40.
599 https://doi.org/10.1016/j.compscitech.2017.06.009
600 Al-Saleh, M.H., 2015. Effect of clay addition on the properties of carbon nanotubes-filled
601 immiscible polyethylene/polypropylene blends. J. Macromol. Sci. Part B Phys. 54,
602 1259–1266. https://doi.org/10.1080/00222348.2015.1085753
603 Alshammari, B.A., Wilkinson, A., 2016. Impact of carbon nanotubes addition on electrical,
604 thermal, morphological, and tensile properties of poly (ethylene terephthalate). Appl.
605 Petrochemical Res. 6, 257–267. https://doi.org/10.1007/s13203-016-0161-2
606 Anbusagar, N.R.R., Palanikumar, K., Ponshanmugakumar, A., 2018. Preparation and
607 properties of nanopolymer advanced composites: A review, in: Jawaid, M., Khan, M.M.
608 (Eds.), Polymer-Based Nanocomposites for Energy and Environmental Applications.
609 Woodhead Publishing Series in Composites Science and Engineering, pp. 27–73.
610 https://doi.org/10.1016/B978-0-08-102262-7.00002-7
611 Arjmandi, R., Hassan, A., Eichhorn, S.J., Mohamad Haafiz, M.K., Zakaria, Z., Tanjung, F.A.,
612 2015a. Enhanced ductility and tensile properties of hybrid montmorillonite/cellulose
613 nanowhiskers reinforced polylactic acid nanocomposites. J. Mater. Sci. 50, 3118–3130.
614 https://doi.org/10.1007/s10853-015-8873-8
615 Arjmandi, R., Hassan, A., Haafiz, M.K.M., Zakaria, Z., 2015b. Partial replacement effect of
616 montmorillonite with cellulose nanowhiskers on polylactic acid nanocomposites. Int. J.
617 Biol. Macromol. 81, 91–99. https://doi.org/10.1016/j.ijbiomac.2015.07.062

618 Arjmandi, R., Hassan, A., Haafiz, M.K.M., Zakaria, Z., Inuwa, I.M., 2014. Characterization
619 of polylactic acid/microcrystalline cellulose/montmorillonite hybrid composites.
620 Malaysian J. Anal. Sci. 18, 642–650.
621 Azam, M.U., Samad, M.A., 2018. UHMWPE hybrid nanocomposite coating reinforced with
622 nanoclay and carbon nanotubes for tribological applications under water with/without
623 abrasives. Tribol. Int. 124, 145–155. https://doi.org/10.1016/j.triboint.2018.04.003
624 Bai, T., Zhu, B., Liu, H., Wang, Y., Song, G., Liu, C., Shen, C., 2020. Biodegradable
625 poly(lactic acid) nanocomposites reinforced and toughened by carbon nanotubes/clay
626 hybrids. Int. J. Biol. Macromol. 151, 628–634.
627 https://doi.org/10.1016/j.ijbiomac.2020.02.209
628 Barrau, S., Vanmansart, C., Moreau, M., Addad, A., Stoclet, G., Lefebvre, J.M., Seguela, R.,
629 2011. Crystallization behavior of carbon nanotube-polylactide nanocomposites.
630 Macromolecules 44, 6496–6502. https://doi.org/10.1021/ma200842n
631 Bhattacharya, M., 2016. Polymer nanocomposites-A comparison between carbon nanotubes,
632 graphene, and clay as nanofillers. Materials (Basel). 9, 262.
633 https://doi.org/10.3390/ma9040262
634 Bilotti, E., Zhang, H., Deng, H., Zhang, R., Fu, Q., Peijs, T., 2013. Controlling the dynamic
635 percolation of carbon nanotube based conductive polymer composites by addition of
636 secondary nanofillers: The effect on electrical conductivity and tuneable sensing
637 behaviour. Compos. Sci. Technol. 74, 85–90.
638 https://doi.org/10.1016/j.compscitech.2012.10.008
639 Chattopadhyay, P.K., Basuli, U., Chattopadhyay, S., 2009. Studies on novel dual filler based
640 epoxidized natural rubber nanocomposite. Polym. Compos. 835–846.
641 https://doi.org/10.1002/pc.20866
642 Chiu, F., 2017. Poly(vinylidene fluoride)/polycarbonate blend-based nanocomposites with

643 enhanced rigidity - Selective localization of carbon nanofillers and organoclay. Polym.
644 Test. 62, 115–123.
645 https://doi.org/http://dx.doi.org/10.1016/j.polymertesting.2017.06.018
646 Choksi, N., Desai, H., 2017. Synthesis of biodegradable polylactic acid polymer by using
647 lactic acid monomer. Int. J. Appl. Chem. 13, 377–384.
648 https://doi.org/https://www.ripublication.com/ijac17/ijacv13v2_19.pdf
649 Chu, C.C., Liu, P., White, K.L., Sue, H.J., 2012. Electrical conductivity and thermal stability
650 of polypropylene containing disentangled carbon nanotubes. Carbon N. Y. 50, 4711–
651 4722. https://doi.org/10.1016/j.carbon.2012.05.063
652 Duman, O., Tunç, S., 2009. Electrokinetic and rheological properties of Na-bentonite in some
653 electrolyte solutions. Microporous Mesoporous Mater. 117, 331–338.
654 https://doi.org/10.1016/j.micromeso.2008.07.007
655 Enotiadis, A., Litina, K., Gournis, D., Rangou, S., Avgeropoulos, A., Xidas, P.,
656 Triantafyllidis, K., 2013. Nanocomposites of polystyrene-b-poly(isoprene)-b-
657 polystyrene triblock copolymer with clay-carbon nanotube hybrid nanoadditives. J.
658 Phys. Chem. B 117, 907–915. https://doi.org/10.1021/jp309361b
659 Francisco, D.L., Paiva, L.B., Aldeia, W., 2018. Advances in polyamide nanocomposites: A
660 review. Polym. Compos. 40, 851–870. https://doi.org/10.1002/pc.24837
661 Fu, L., Wu, F., Xu, C., Cao, T., Wang, R., Guo, S., 2018. Anisotropic shape memory
662 behaviors of polylactic Acid/Citric Acid– bentonite composite with a gradient filler
663 concentration in thickness direction. Ind. Eng. Chem. Res. 57, 6265–6274.
664 https://doi.org/10.1021/acs.iecr.8b00602
665 Galimberti, M., Coombs, M., Pandini, S., Riccò, T., Cipolletti, V., Conzatti, L., Guerra, G.,
666 2015. Delamination of organically modified montmorillonite for reducing the filler
667 networking with carbon black in poly(1,4-cis-isoprene) based nanocomposites. Appl.

668 Clay Sci. 104, 8–17. https://doi.org/10.1016/j.clay.2014.11.017
669 Garcia, N.L., Fama, L., D'Accorso, N.B., Goyanes, S., 2015. Biodegradable starch
670 nanocomposites, in: Thakur, V.K., Thakur, M.K. (Eds.), Eco-friendly polymer
671 nanocomposites processing and properties. Springer, India, pp. 17–77.
672 https://doi.org/10.1007/978-81-322-2470-9_2
673 Geng, C., Wang, J., Zhang, Q., Fu, Q., 2012. New piezoelectric damping composites of
674 poly(vinylidene fluoride) blended with clay and multi-walled carbon nanotubes. Polym.
675 Int. 61, 934–938. https://doi.org/10.1002/pi.4161
676 Gorrasi, G., D'Ambrosio, S., Patimo, G., Pantani, R., 2014. Hybrid clay-carbon
677 nanotube/PET composites: Preparation, processing, and analysis of physical properties.
678 J. Appl. Polym. Sci. 131, 1–7. https://doi.org/10.1002/app.40441
679 Gorrasi, G., Milone, C., Piperopoulos, E., Lanza, M., Sorrentino, A., 2013. Hybrid clay
680 mineral-carbon nanotube-PLA nanocomposite films. Preparation and photodegradation
681 effect on their mechanical, thermal and electrical properties. Appl. Clay Sci. 71, 49–54.
682 https://doi.org/10.1016/j.clay.2012.11.004
683 Guadagno, L., De Vivo, B., Di Bartolomeo, A., Lamberti, P., Sorrentino, A., Tucci, V.,
684 Vertuccio, L., Vittoria, V., 2011. Effect of functionalization on the thermo-mechanical
685 and electrical behavior of multi-wall carbon nanotube/epoxy composites. 49, 1919–
686 1930. Carbon N. Y. https://doi.org/10.1016/j.carbon.2011.01.017
687 Ha, C.S., 2006. Poly(butylene terephthlate) (PBT) based nanocomposites, in: Mai, Y.-W.,
688 Yu, Z.-Z. (Eds.), Polymer nanocomposites. Woodhead Publishing, England, pp. 234–
689 255.
690 Hapuarachchi, T.D., Peijs, T., 2010. Multiwalled carbon nanotubes and sepiolite nanoclays as
691 flame retardants for polylactide and its natural fibre reinforced composites. Compos.
692 Part A Appl. Sci. Manuf. 41, 954–963.

https://doi.org/10.1016/j.compositesa.2010.03.004

Hosseini, S.M., Yousefi, A.A., 2017. Electrospun PVDF/MWCNT/OMMT hybrid nanocomposites: preparation and characterization. Iran. Polym. J. 26, 331–339. https://doi.org/10.1007/s13726-017-0522-4

Hu, C., Li, Z., Wang, Y., Gao, J., Dai, K., Zheng, G., 2017. Comparative assessment of the strain-sensing behaviors of polylactic acid nanocomposites: reduced graphene oxide or carbon nanotubes. J. Mater. Chem. C 5, 2318–2328. https://doi.org/10.1039/c6tc05261d

Huang, Z., Wan, Y., Peng, M., Yang, Z., Luo, H., 2020. Incorporating nanoplate-like hydroxyapatite into polylactide for biomimetic nanocomposites via direct melt intercalation. Compos. Sci. Technol. 185, 107903. https://doi.org/10.1016/j.compscitech.2019.107903

Jain, S., 2012. Development of an antibody functionalized carbon nanotube biosensor for foodborne bacterial pathogens. J. Biosens. Bioelectron. 11, 002. https://doi.org/10.4172/2155-6210.s11-002

Jia, L., Zhang, W., Tong, B., Yang, R., 2019. Crystallization, flame-retardant, and mechanical behaviors of poly(lactic acid)\9,10-dihydro-9-oxa-10-phosphaphenanthrene-10-oxide–calcium montmorillonite nanocomposite. J. Appl. Polym. Sci. 136, 46982. https://doi.org/10.1002/app.46982

Katiyar, V., Gerds, N., Koch, C.B., Risbo, J., Hansen, H.C.B., Plackett, D., 2010. Poly l-lactide-layered double hydroxide nanocomposites via in situ polymerization of l-lactide. Polym. Degrad. Stab. 95, 2563–2573. https://doi.org/10.1016/j.polymdegradstab.2010.07.031

Keshavarzi, S., Babaei, A., Goudarzi, A., Shakeri, A., 2019. ZnO nanoparticles as chain elasticity reducer and structural elasticity enhancer: Correlating the degradating role and localization of ZnO with the morphological and mechanical properties of PLA/PP/ZnO

718 nanocomposite. Polym. Adv. Technol. 30, 1083-1095. https://doi.org/10.1002/pat.4542
719 Khajehpour, M., Arjmand, M., Sundararaj, U., 2014. Dielectric properties of multiwalled
720 carbon nanotube/ clay/polyvinylidene fluoride nanocomposites: effect of clay
721 incorporation. Polym. Compos. 37, 161–167. https://doi.org/10.1002/pc.23167
722 Koo, J., 2016. Environmental and health impacts for nanomaterials and polymer
723 nanocomposites, in: Koo, J. (Ed.), Fundamentals, properties, and applications of
724 polymer nanocomposites. Cambridge University Press, Cambridge, pp. 605–647.
725 https://doi.org/10.1017/cbo9781139342766.015
726 Kumar, A., Kumar, K., Ghosh, P.K., Yadav, K.L., 2018. MWCNT/TiO_2 hybrid nano filler
727 toward high-performance epoxy composite. Ultrason. Sonochem. 41, 37–46.
728 https://doi.org/10.1016/j.ultsonch.2017.09.005
729 Lee, J., Kim, M., Hong, C.K., Shim, S.E., 2007. Measurement of the dispersion stability of
730 pristine and surface-modified multiwalled carbon nanotubes in various nonpolar and
731 polar solvents. Meas. Sci. Technol. 18, 3707–3712. https://doi.org/10.1088/0957-
732 0233/18/12/005
733 Levchenko, V., Mamunya, Y., Boiteux, G., Lebovka, M., Alcouffe, P., Seytre, G., Lebedev,
734 E., 2011. Influence of organo-clay on electrical and mechanical properties of
735 PP/MWCNT/OC nanocomposites. Eur. Polym. J. 47, 1351–1360.
736 https://doi.org/10.1016/j.eurpolymj.2011.03.012
737 Liu, S., Wu, G., Chen, X., Zhang, X., Yu, J., Liu, M., Zhang, Y., Wang, P., 2019.
738 Degradation behavior in vitro of carbon nanotubes (CNTs)/poly(lactic acid) (PLA)
739 composite suture. Polymers (Basel). 11. https://doi.org/10.3390/polym11061015
740 Liu, Y., Wang, S., Lan, W., Qin, W., 2019. Fabrication of polylactic acid/carbon
741 nanotubes/chitosan composite fibers by electrospinning for strawberry preservation. Int.
742 J. Biol. Macromol. 121, 1329–1336. https://doi.org/10.1016/j.ijbiomac.2018.09.042

743 Lv, S., Zhang, Y., Tan, H., 2019. Thermal and thermo-oxidative degradation kinetics and
744 characteristics of poly (lactic acid) and its composites. Waste Manag. 87, 335–344.
745 https://doi.org/10.1016/j.wasman.2019.02.027
746 Ma, H., Tong, L., Xu, Z., Fang, Z., 2007. Synergistic effect of carbon nanotube and clay for
747 improving the flame retardancy of ABS resin. Nanotechnology 18, 375602.
748 https://doi.org/10.1088/0957-4484/18/37/375602
749 Ma, R., Zhu, B., Zeng, Q., Wang, P., Wang, Y., Liu, C., Shen, C., 2019. Melt-processed
750 poly(ether ether ketone)/carbon nanotubes/montmorillonite nanocomposites with
751 enhanced mechanical and thermomechanical properties. Materials (Basel). 12, 1–14.
752 https://doi.org/10.3390/ma12030525
753 Madaleno, L., Pyrz, R., Crosky, A., Jensen, L.R., Rauhe, J.C.M., Dolomanova, V., Timmons,
754 A.M.M.V. de B., Pinto, J.J.C., Norman, J., 2013. Processing and characterization of
755 polyurethane nanocomposite foam reinforced with montmorillonite-carbon nanotube
756 hybrids. Compos. Part A Appl. Sci. Manuf. 44, 1–7.
757 https://doi.org/10.1016/j.compositesa.2012.08.015
758 Madaleno, L., Pyrz, R., Jensen, L.R., Pinto, J.J.C., Lopes, A.B., Dolomanova, V., Schjødt-
759 Thomsen, J., Rauhe, J.C.M., 2012. Synthesis of clay-carbon nanotube hybrids: Growth
760 of carbon nanotubes in different types of iron modified montmorillonite. Compos. Sci.
761 Technol. 72, 377–381. https://doi.org/10.1016/j.compscitech.2011.11.027
762 Malkappa, K., Bandyopadhyay, J., Ray, S.S., 2018. Thermal degradation characteristic and
763 flame retardancy of polylactide-based nanobiocomposites. Molecules 23, 2648.
764 https://doi.org/10.3390/molecules23102648
765 Manikandan, D., Mangalaraja, R.V., Avila, R.E., Siddheswaran, R., Ananthakumar, S., 2012.
766 Carbon nanotubes rooted montmorillonite (CNT-MM) reinforced nanocomposite
767 membrane for PEM fuel cells. Mater. Sci. Eng. B Solid-State Mater. Adv. Technol. 177,

614–618. https://doi.org/10.1016/j.mseb.2012.02.027

Manikandan, D., Viswanathan, R., Avila, R.E., Siddheswaran, R., Anathakumar, S., 2013. Montmorillonite – carbon nanotube nanofillers by acetylene decomposition using catalytic CVD. Appl. Clay Sci. 71, 37–41. https://doi.org/10.1016/j.clay.2012.10.001

Mishra, R.K., Mohanty, K., 2018. Pyrolysis kinetics and thermal behavior of waste sawdust biomass using thermogravimetric analysis. Bioresour. Technol. 251, 63–74. https://doi.org/10.1016/j.biortech.2017.12.029

Molinaro, S., Cruz Romero, M., Boaro, M., Sensidoni, A., Lagazio, C., Morris, M., Kerry, J., 2013. Effect of nanoclay-type and PLA optical purity on the characteristics of PLA-based nanocomposite films. J. Food Eng. 117, 113–123. https://doi.org/10.1016/j.jfoodeng.2013.01.021

Montanheiro, T.L.D.A., Cristóvan, F.H., Machado, J.P.B., Tada, D.B., Durán, N., Lemes, A.P., 2015. Effect of MWCNT functionalization on thermal and electrical properties of PHBV/MWCNT nanocomposites. J. Mater. Res. 30, 55–65. https://doi.org/10.1557/jmr.2014.303

Mumtazah, Z., Priyangga, A., Atmaja, L., 2019. Some properties of membrane based on chitosan/phthalic anhydride matrices using montmorillonite/multi-walled carbon nanotubes filler for DMFC application Some properties of membrane based on chitosan/phthalic anhydride matrices using montmorillonite / m, in: International Conference on Science and Applied Science (ICSAS). Indonesia, pp. 1–6. https://doi.org/https://doi.org/10.1063/1.5141679

Narro-Céspedes, R.I., Neira-Velázquez, M.G., Mora-Cortes, L.F., Hernández-Hernández, E., Castañeda-Facio, A.O., Ibarra-Alonso, M.C., Reyes-Acosta, Y.K., Soria-Arguello, G., Borjas-Ramos, J.J., 2018. Surface modification of sodium montmorillonite nanoclay by plasma polymerization and its effect on the properties of polystyrene nanocomposites. J.

793 Nanomater. 2018, 2480798. https://doi.org/10.1155/2018/2480798
794 Niu, S., Zhou, Y., Yu, H., Lu, C., Han, K., 2017. Investigation on thermal degradation
795 properties of oleic acid and its methyl and ethyl esters through TG-FTIR. Energy
796 Convers. Manag. 149, 495–504. https://doi.org/10.1016/j.enconman.2017.07.053
797 Norazlina, H., Hadi, A.A., Qurni, A.U., Amri, M., Mashelmie, S., Kamal, Y., 2019. Effects
798 of multi-walled carbon nanotubes (MWCNTs) on the degradation behavior of
799 plasticized PLA nanocomposites. Polym. Bull. 76, 1453–1469.
800 https://doi.org/10.1007/s00289-018-2454-3
801 Pan, H., Pan, Y., Wang, W., Song, L., Hu, Y., Liew, K.M., 2014. Synergistic effect of layer-
802 by-layer assembled thin films based on clay and carbon nanotubes to reduce the
803 flammability of flexible polyurethane foam. Ind. Eng. Chem. Res. 53, 14315–14321.
804 https://doi.org/10.1021/ie502215p
805 Pandey, P., Mohanty, S., Nayak, S.K., 2014. Improved flame retardancy and thermal stability
806 of polymer/clay nanocomposites, with the incorporation of multiwalled carbon nanotube
807 as secondary filler: Evaluation of hybrid effect of nanofillers. High Perform. Polym. 26,
808 826–836. https://doi.org/10.1177/0954008314531802
809 Pires, M., Murariu, M., Cardoso, A.M., Bonnaud, L., Dubois, P., 2020. Thermal degradation
810 of poly(lactic acid)–zeolite composites produced by melt-blending. Polym. Bull. 77,
811 2111–2137. https://doi.org/10.1007/s00289-019-02846-4
812 Qin, Y., Wang, W., Zhang, H., Dai, Y., Hou, H., Dong, H., 2018. Effects of organic
813 modification of montmorillonite on the properties of hydroxypropyl di-starch phosphate
814 films prepared by extrusion blowing. Materials (Basel). 11, 1064.
815 https://doi.org/10.3390/ma11071064
816 Raji, M., Mekhzoum, M.E.M., Qaiss, A.K., Bouhfid, R., 2016. Nanoclay modification and
817 functionalization for nanocomposites development: Effect on the structural,

morphological, mechanical and rheological properties, in: Jawaid, M., Qaiss, A., Bouhfid, R. (Eds.), Nanoclay reinforced polymer composites, engineering materials. Springer, Singapore, pp. 1–34. https://doi.org/10.1007/978-981-10-1953-1

Raji, M., Mekhzouma, M.M., Rodrigue, D., Qaissa, A., Bouhfi, R., 2018. Effect of silane functionalization on properties of polypropylene/clay nanocomposites. Compos. Part B 146, 106–115. https://doi.org/10.1016/j.compositesb.2018.04.013

Ramírez-Herrera, C.A., Gonzalez, H., de la Torre, F., Benitez, L., Cabañas-Moreno, J., Lozano, K., 2019. Electrical properties and electromagnetic interference shielding effectiveness of interlayered systems composed by carbon nanotube filled carbon nanofiber mats and polymer composites. Nanomaterials 9, 1–19. https://doi.org/10.3390/nano9020238

Santangelo, S., Gorrasi, G., Di Lieto, R., De Pasquale, S., Patimo, G., Piperopoulos, E., Lanza, M., Faggio, G., Mauriello, F., Messina, G., Milone, C., 2011. Polylactide and carbon nanotubes/smectite-clay nanocomposites: Preparation, characterization, sorptive and electrical properties. Appl. Clay Sci. 53, 188–194. https://doi.org/10.1016/j.clay.2010.12.013

Sanusi, O.M., Benelfellah, A., Aït Hocine, N., 2020a. Clays and carbon nanotubes as hybrid nanofillers in thermoplastic-based nanocomposites – A review. Appl. Clay Sci. 185, 105408. https://doi.org/10.1016/j.clay.2019.105408

Sanusi, O.M., Papadopoulos, L., Klonos, P.A., Terzopoulou, Z., Aït Hocine, N., Benelfellah, A., Papageorgiou, G.Z., Kyritsis, A., Bikiaris, D.N., 2020b. Calorimetric and dielectric study of renewable poly(hexylene 2,5-furan-dicarboxylate)-based nanocomposites in situ filled with small amounts of graphene platelets and silica nanoparticles. Polymers. 12, 1239. https://doi.org/10.3390/POLYM12061239

Shabanian, M., Hajibeygi, M., Hedayati, K., Khaleghi, M., Khonakdar, H.A., 2016. New

ternary PLA/organoclay-hydrogel nanocomposites: Design, preparation and study on thermal, combustion and mechanical properties. Mater. Des. 110, 811–820. https://doi.org/10.1016/j.matdes.2016.08.059

Shayan, M., Azizi, H., Ghasemi, I., Karrabi, M., 2019. Influence of modified starch and nanoclay particles on crystallization and thermal degradation properties of cross-linked poly(lactic acid). J. Polym. Res. 26. https://doi.org/10.1007/s10965-019-1879-1

Sianipar, M., Kim, S.H., Khoiruddin, Iskandar, F., Wenten, I.G., 2017. Functionalized carbon nanotube (CNT) membrane: Progress and challenges. RSC Adv. 7, 51175–51198. https://doi.org/10.1039/c7ra08570b

Sibeko, M.A., 2012. Preparation and characterization of vinylsilane crosslinked high-density polyethylene composites filled with nanoclays. University of The Free State. https://doi.org/10.1002/pc.22575

Song, S.H., 2016. Synergistic effect of clay platelets and carbon nanotubes in styrene–butadiene rubber nanocomposites. Macromol. Chem. Phys. 217, 2617–2625. https://doi.org/10.1002/macp.201600344

Stern, N., Dyamant, I., Shemer, E., Hu, X., Marom, G., 2018. Hybrid effects in the fracture toughness of polyvinyl butyral-based nanocomposites. Nanocomposites 4, 1–9. https://doi.org/10.1080/20550324.2018.1447827

Terzopoulou, Z., Bikiaris, D.N., Triantafyllidis, K.S., Potsi, G., Gournis, D., Papageorgiou, G.Z., Rudolf, P., 2016. Mechanical, thermal and decomposition behavior of poly(ε-caprolactone) nanocomposites with clay-supported carbon nanotube hybrids. Thermochim. Acta 642, 67–80. https://doi.org/10.1016/j.tca.2016.09.001

Terzopoulou, Z., Klonos, P.A., Kyritsis, A., Tziolas, A., Avgeropoulos, A., Papageorgiou, G.Z., Bikiaris, D.N., 2019a. Interfacial interactions, crystallization and molecular mobility in nanocomposites of Poly(lactic acid) filled with new hybrid inclusions based

on graphene oxide and silica nanoparticles. Polymer. 166, 1–12. https://doi.org/10.1016/j.polymer.2019.01.041

Terzopoulou, Z., Tarani, E., Kasmi, N., Papadopoulos, L., Chrissafis, K., Papageorgiou, D.G., Papageorgiou, G.Z., Bikiaris, D.N., 2019b. Thermal decomposition kinetics and mechanism of In-Situ Prepared Bio-Based Poly(propylene 2,5-furan dicarboxylate)/Graphene Nanocomposites. Molecules 24, 1717. https://doi.org/10.3390/molecules24091717

Timochenco, L., Grassi, V.G., Dal Pizzol, M., Costa, J.M., Castellares, L.G., Sayer, C., Machado, R.A.F., Araújo, P.H.H., 2010. Swelling of organoclays in styrene. Effect on flammability in polystyrene nanocomposites. Express Polym. Lett. 4, 500–508. https://doi.org/10.3144/expresspolymlett.2010.63

Tunç, S., Duman, O., 2011. Preparation of active antimicrobial methyl cellulose/carvacrol/montmorillonite nanocomposite films and investigation of carvacrol release. LWT - Food Sci. Technol. 44, 465–472. https://doi.org/10.1016/j.lwt.2010.08.018

Tunç, S., Duman, O., 2010. Preparation and characterization of biodegradable methyl cellulose/montmorillonite nanocomposite films. Appl. Clay Sci. 48, 414–424. https://doi.org/10.1016/j.clay.2010.01.016

Vennerberg, D., Hall, R., Kessler, M.R., 2014. Supercritical carbon dioxide-assisted silanization of multi-walled carbon nanotubes and their effect on the thermo-mechanical properties of epoxy nanocomposites. Polymer. 55, 4156–4163. https://doi.org/10.1016/j.polymer.2014.06.020

Vukić, N., Ristić, I.S., Marinović-Cincović, M., Radičević, R., Pilić, B., Cakić, S., Budinski-Simendić, J., 2019. Influence of different functionalization methods of multi-walled carbon nanotubes on the properties of poly(L-lactide) based nanocomposites. Hem. Ind.

73, 183–196. https://doi.org/10.2298/HEMIND190402016V

Wang, Z., Meng, X., Li, J., Du, X., Li, S., Jiang, Z., Tang, T., 2009. A simple method for preparing carbon nanotubes/clay hybrids in water. J. Phys. Chem. C 113, 8058–8064. https://doi.org/10.1021/jp811260p

Wu, W., Liu, T., Zhang, D., Sun, Q., Cao, K., Zha, J., Lu, Y., Wang, B., Cao, X., Feng, Y., Roy, V.A.L., Li, R.K.Y., 2019. Significantly improved dielectric properties of polylactide nanocomposites via TiO_2 decorated carbon nanotubes. Compos. Part A Appl. Sci. Manuf. 127, 105650. https://doi.org/10.1016/j.compositesa.2019.105650

Yang, T., Wu, D., Lu, L., Zhou, W., Zhang, M., 2011. Electrospinning of polylactide and its composites with carbon nanotubes. Polym. Compos. 32, 1280–1288. https://doi.org/10.1002/pc.21149

Yang, S., Wu, Z., Yang, W., Yang, M., 2008. Thermal and mechanical properties of chemical crosslinked polylactide (PLA). Polym. Test. 27, 957–963. https://doi.org/10.1016/j.polymertesting.2008.08.009

Zhang, W.-D., Phang, I.Y., Liu, T., 2006. Growth of carbon nanotubes on clay: unique nanostructured filler for high-performance polymer nanocomposites. Adv. Mater. 18, 73–77. https://doi.org/10.1002/adma.200501217

Zhang, X., Xu, R., Wu, Z., Zhou, C., 2003. The synthesis and characterization of polyurethane/clay nanocomposites. Polym. Int. 52, 790–794. https://doi.org/10.1002/pi.1152

Zhou, Y., Lei, L., Yang, B., Li, J., Ren, J., 2018. Preparation and characterization of polylactic acid (PLA) carbon nanotube nanocomposites. Polym. Test. 68, 34–38. https://doi.org/10.1016/j.polymertesting.2018.03.044

Zhu, B., Bai, T., Wang, P., Wang, Y., Liu, C., Shen, C., 2020. Selective dispersion of carbon nanotubes and nanoclay in biodegradable poly(ε-caprolactone)/poly(lactic acid) blends

with improved toughness, strength and thermal stability. Int. J. Biol. Macromol. 153, 1272–1280. https://doi.org/10.1016/j.ijbiomac.2019.10.262

Zhu, W., Miser, D.E., Chan, W.G., Hajaligol, M.R., 2004. Characterization of combustion fullerene soot, C60, and mixed fullerene. Carbon N. Y. 42, 1463–1471. https://doi.org/10.1016/j.carbon.2004.01.076

Zhuang, G., Zhang, Z., Guo, J., Liao, L., Zhao, J., 2015. A new ball milling method to produce organo-montmorillonite from anionic and nonionic surfactants. Appl. Clay Sci. 104, 18–26. https://doi.org/10.1016/j.clay.2014.11.023

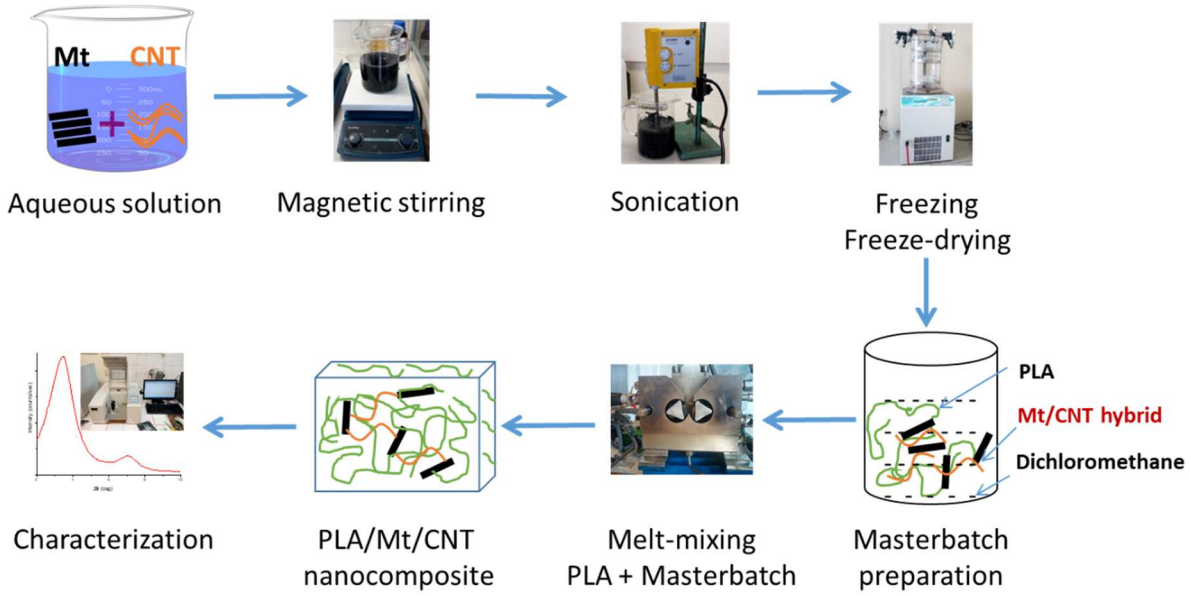
Mt
CNT
Aqueous solution
Magnetic stirring
Sonication
Freezing
Freeze-drying
PLA
Mt/CNT hybrid
Dichloromethane
Masterbatch
preparation
Melt-mixing
PLA + Masterbatch
PLA/Mt/CNT
nanocomposite
Characterization